BIOCHEMISTRY
including biophysical chemistry & molecular biology
Article

Biochemistry **2011,** *50,* 1001–1015 1001
DOI: 10.1021/bi101822y

Sulfated Glycosaminoglycans Accelerate Transthyretin Amyloidogenesis by Quaternary Structural Conversion†

Steve Bourgault,‡ James P. Solomon,‡ Natàlia Reixach,§ and Jeffery W. Kelly*,‡,§

‡*Department of Chemistry and The Skaggs Institute for Chemical Biology and* §*Department of Molecular and Experimental Medicine, The Scripps Research Institute, 10550 North Torrey Pines Road, La Jolla, California, 92037*

Received November 12, 2010; Revised Manuscript Received December 30, 2010

ABSTRACT: Glycosaminoglycans (GAGs), which are found in association with all extracellular amyloid deposits in humans, are known to accelerate the aggregation of various amyloidogenic proteins *in vitro*. However, the precise molecular mechanism(s) by which GAGs accelerate amyloidogenesis remains elusive. Herein, we show that sulfated GAGs, especially heparin, accelerate transthyretin (TTR) amyloidogenesis by quaternary structural conversion. The clustering of sulfate groups on heparin and its polymeric nature are essential features for accelerating TTR amyloidogenesis. Heparin does not influence TTR tetramer stability or TTR dissociation kinetics, nor does it alter the folded monomer−misfolded monomer equilibrium directly. Instead, heparin accelerates the conversion of preformed TTR oligomers into larger aggregates. The more rapid disappearance of monomeric TTR in the presence of heparin likely reflects the fact that the monomer−misfolded amyloidogenic monomer−oligomer−TTR fibril equilibria are all linked, a hypothesis that is strongly supported by the light scattering data. TTR aggregates prepared in the presence of heparin exhibit a higher resistance to trypsin and proteinase K proteolysis and a lower exposure of hydrophobic side chains comprising hydrophobic clusters, suggesting an active role for heparin in amyloidogenesis. Our data suggest that heparin accelerates TTR aggregation by a scaffold-based mechanism, in which the sulfate groups comprising GAGs interact primarily with TTR oligomers through electrostatic interactions, concentrating and orienting the oligomers, facilitating the formation of higher molecular weight aggregates. This model raises the possibility that GAGs may play a protective role in human amyloid diseases by interacting with proteotoxic oligomers and promoting their association into less toxic amyloid fibrils.

The aberrant assembly of one of more than 25 human proteins into diverse cross-β-sheet quaternary structures is the hallmark of human amyloid diseases, including Alzheimer's disease, the transthyretin amyloidoses, and the light chain amyloidoses (*1*−*5*). Amyloid diseases differ by the protein deposited in the extracellular space and the specific tissues subjected to deposition and degeneration (*2*, *5*, *6*). The causative link between amyloidogenesis and the observed pathology is supported by compelling genetic and biochemical evidence (*1*, *2*, *6*−*8*). Although the exact molecular structure(s) of the proteotoxic species and the mechanism(s) of proteotoxicity are still unclear, cell and animal model studies of several amyloidogenic proteins suggest that the oligomers, which may or may not be on pathway to fibril formation, are more deleterious than mature fibrils (*9*−*13*). Amyloid fibrils share several common features, such as an extensive cross-β-sheet structure and the ability to selectively bind thioflavin T (ThT)[1] and Congo Red. Amyloid fibrils and a subset of oligomers also associate with nonfibrillar accessory molecules, including the serum amyloid P component (*14*), apolipoprotein E (*15*), and collagen (*16*). In addition, glycosaminoglycans ubiquitously associate with all amyloid deposits (*17*), including those from transthyretin (*18*, *19*), Aβ (*20*), β_2-microglobulin (*21*), immunoglobulin light chain (*22*), and islet amyloid polypeptide (IAPP) (*23*).

Glycosaminoglycans (GAGs) are long unbranched polysaccharides consisting of disaccharide repeating subunits. They are abundant in the extracellular matrix (ECM) of multicellular organisms, where they can be found either covalently linked to the protein core of proteoglycans or as free macromolecules. Biophysical investigations have shown that GAGs, particularly heparan sulfate (HS) and its highly sulfated derivative heparin, promote or accelerate aggregation of the prion protein (*24*), gelsolin (*25*), immunoglobulin light chain (*26*), Aβ (*27*), α-synuclein (*28*), β_2-microglobulin (*29*), and IAPP (*30*). However, mechanistic insight is sparse. It has been suggested that heparin can accelerate muscle acylphosphatase (mAcP) aggregation through a scaffold-based mechanism, in which mAcP monomers interact with the sulfate moieties of the heparin molecule, increasing the local concentration of and orienting mAcP, promoting its oligomerization (*31*). Consistent with this hypothesis, HS and/or heparin favors the formation of β_2-microglobulin oligomers (*32*). Moreover, GAGs induce amyloid fibril extension of β_2-microglobulin (*33*) and stabilize the fibrils upon their formation (*34*),

†This research was generously supported by the National Institutes of Health (DK46335), The Skaggs Institute for Chemical Biology, and the Lita Annenberg Hazen Foundation. S.B. is a recipient of a postdoctoral fellowship from the Fonds de la Recherche en Santé du Québec (FRSQ).

*To whom correspondence should be addressed. Phone: (858) 784-9880. Fax: (858) 784-9610. E-mail: jkelly@scripps.edu.

[1]Abbreviations: Aβ, amyloid-β; ANS, 8-anilinonaphthalene-1-sulfonate; CD, circular dichroism; CNBr, cyanogen bromide; CNSA, central nervous system selective amyloidosis; ECM, extracellular matrix; FAC, familial amyloid cardiomyopathy; FAP, familial amyloidotic polyneuropathy; GAG, glycosaminoglycan; GdnCl, guanidinium chloride; GlcN, glucosamine; HS, heparan sulfate; IAPP, islet amyloid polypeptide; IdoA, iduronic acid; mAcP, muscle acylphosphatase; SSA, senile systemic amyloidosis; ThT, thioflavin T; TTR, transthyretin; WT, wild type.

Published on Web 12/31/2010

inhibiting their depolymerization (*35*). Recently, it has been suggested that HS accelerates the conversion of monomeric mAcP from its native state into a partially unfolded monomeric intermediate and this intermediate into oligomers (*36*). GAGs have also been shown to accelerate the transition of serum amyloid A protein (*37*), gelsolin (*25*), and Aβ (*27*) from random coil to β-sheet, a structural modification most likely related to the aggregation process rather than to a conformational change within the monomeric protein. These studies emphasize that the precise molecular mechanism by which GAGs accelerate amyloidogenesis remains elusive, meriting significant effort since amyloid fibril formation in humans is inextricably linked to GAG binding (*16*, *17*).

The transthyretin (TTR) amyloid diseases are characterized by the extracellular aggregation of either wild-type (WT) or mutant TTR (*38*, *39*). TTR is a 55 kDa tetrameric protein composed of 127-residue β-sheet-rich subunits (*40*, *41*) and is mainly synthesized by the liver and the choroid plexus (*42*). TTR circulates in plasma and cerebrospinal fluid, where it acts as a carrier of thyroxine and holo-retinol-binding protein (*42*). The aggregation of TTR is linked to the degeneration of specific tissues, especially postmitotic tissues, including the peripheral nervous system and the heart (*38*, *39*). Senile systemic amyloidosis (SSA), associated with age-onset deposition of WT TTR in the heart, gut, lung, and carpal tunnel, often leads to congestive heart failure (*43*). More than 100 amyloidogenic TTR mutants have been described (*44*) that are associated with autosomal dominant degenerative disorders, including familial amyloidotic polyneuropathy (FAP) linked to the degradation of the peripheral nervous system (*38*), familial amyloid cardiomyopathy (FAC) (*39*) compromising cardiac function, and the rare central nervous system selective amyloidosis (CNSA) (*45*). FAP and FAC exhibit an earlier onset than SSA, with the most aggressive variants exhibiting clinical manifestations during the second decade of life (*46*).

The mechanism by which TTR forms amyloid fibrils has been characterized *in vitro* (*47*, *48*). This process, which also appears to operate *in vivo*, initially involves the dissociation of the native tetramer into constituent monomers (*49*), the rate-limiting step of amyloidogenesis (*50*, *51*). Partial denaturation of the released monomer is required (*52*) to allow the formation of oligomers, soluble aggregates, insoluble aggregates, and, eventually, amyloid fibrils through a downhill polymerization process (*53*). Formation of TTR amyloid fibrils is favored by the presence of amyloidogenic mutations in the protein sequence that change the thermodynamic and/or kinetic stability of the TTR tetramer or monomer (*6*, *54*, *55*). The extent of destabilization of the TTR mutants correlates with the severity of the resulting disease (*6*, *54*−*56*), until cellular endoplasmic reticulum-associated degradation begins to predominate, which reduces the concentration of the TTR variant secreted, thus reducing amyloidogenicity (*6*). Designed small molecules that bind to the largely unoccupied thyroxine-binding sites within TTR in blood kinetically stabilize the TTR tetrameric quaternary structure, inhibiting TTR amyloid fibril formation (*40*). One of these, Tafamidis, was recently shown to halt the progression of neurodegeneration associated with FAP in a placebo-controlled clinical trial.

As in other amyloid diseases, the major site of TTR deposition is the ECM. In FAP, the amorphous aggregates and amyloid fibrils are found prominently in the endoneurium of peripheral nerves, where they are surrounded by collagen (*19*, *57*). Nerve biopsies from FAP patients carrying the amyloidogenic V30M mutation showed that TTR fibril extracts contain HS and chondroitin sulfate proteoglycans (*19*). Cardiac TTR deposits found in association with the basement membrane surrounding myocardial cells contain free GAG chains, such as chondroitin sulfate, HS/heparin, and hyaluronan (*18*, *58*).

The tissue-specific deposition of TTR amyloid fibrils in the ECM, the close association of TTR amyloid fibrils with collagen and GAGs, the known resistance of recombinant TTR to aggregate at physiological pH, and the well-known ability of GAGs to promote fibril formation from several other amyloidogenic proteins all suggest that GAGs and other ECM components could play an active role in facilitating TTR amyloidogenesis. Nonetheless, the influence of ECM components on TTR amyloidogenesis has not been investigated so far, nor has the mechanism of the influence of GAGs on TTR amyloidogenesis been explored. Herein, we have investigated the effects of GAGs on TTR aggregation *in vitro*. Our results demonstrate that sulfated GAGs, especially heparin, accelerate TTR aggregation. Mechanistic investigations reveal that heparin induces TTR amyloidogenesis by a scaffold-based mechanism, in which the sulfate moieties of GAGs interact primarily with soluble TTR oligomers, facilitating the formation of higher molecular weight aggregates, including amyloid fibrils, by quaternary structure conversion.

EXPERIMENTAL PROCEDURES

Expression and Purification of TTR. All TTR variants were expressed in BL21(DE3) Epicurian Gold *Escherichia coli* cells (Stratagene, La Jolla, CA). Cells were transformed with pMMHa expression vector containing the appropriate TTR variant and ampicillin resistance genes, and the expression was induced by addition of IPTG to a final concentration of 1 mM (*54*). Cells were grown, harvested, and lysed, and TTR variants were isolated and purified as previously described (*53*). Briefly, cell supernatants were fractionated by ammonium sulfate precipitation, 45−90% pellet for tetrameric TTR variants and a 25−90% pellet for engineered monomeric variants. Ammonium sulfate pellets were resuspended in 25 mM Tris and 1 mM EDTA, pH 8.0, and purified at 4 °C by anion-exchange chromatography employing a Source 15Q anion-exchange column (Amersham Biosciences, Piscataway, NJ). Fractions containing the desired proteins were pooled, concentrated, and further purified at 4 °C on a Superdex 75 gel filtration column (Amersham Biosciences, Piscataway, NJ) in buffer A (10 mM sodium phosphate (pH 7.6), 100 mM KCl, and 1 mM EDTA). The identity and the purity of each purified TTR variant were verified by electrospray mass spectrometry and by SDS−PAGE. Concentrations of TTR solutions were determined by measuring the absorbance at 280 nm, using a molar extinction coefficient of 18450 M^{-1} cm^{-1} for monomeric variants and 73800 M^{-1} cm^{-1} for tetrameric variants.

Aggregation Kinetics Measured by Turbidity. Reactions were initiated by the addition of 2× TTR stock solutions in buffer A to an equivalent volume of 200 mM acetate buffer (100 mM KCl, 1 mM EDTA, pH varying from 4.8 to 6.0) to reach a final protein concentration of 0.2 mg/mL. Assays were performed at 37 °C without stirring (except for an initial 3 s shaking prior to the first measurement) in sealed black-wall, clear-bottom 96-well plates with a total volume of 100 μL per well. The increase of turbidity at 400 nm was measured at intervals of 5 min (unless specified) over the course of 30 h, using a SpectraMax 250

UV−vis plate reader (Molecular Devices, Sunnyvale, CA). GAGs were prepared as a 200× (20 mg/mL to 0.2 mg/mL) stock solution in water and were diluted 1:100 into 2× TTR stock solution, prior to the addition of this solution to an equivalent volume of acetate buffer to reach the desired final concentration of GAGs (1−100 μg/mL) and TTR (0.2 mg/mL). For each experiment, control reactions (without TTR) were carried out. The data obtained from triplicate wells were averaged, corrected by subtracting the corresponding control reaction, and plotted as turbidity vs time. Each curve represents the average of at least three independent experiments performed in triplicate. High molecular weight heparin sodium salt (13−17 kDa) from porcine intestinal mucosa and low molecular weight heparin (3−7 kDa) from porcine intestinal mucosa were purchased from Calbiochem (San Diego, CA). Heparin oligosaccharides (dp8, dp4) and uronic acid-2-sulfate−2-deoxy-2-sulfamido-α-D-glucopyranosyl-6-*O*-sulfate (UA,2S−GlcNS,6S) disaccharide were purchased from Iduron (Manchester, U.K.). Hyaluronic acid sodium salt from bovine vitreous humor, chondroitin sulfate A sodium salt from bovine trachea, chondroitin sulfate C sodium salt from shark cartilage, dermatan sulfate sodium salt from porcine intestinal mucosa, keratan sulfate from bovine cornea, heparin sulfate sodium salt from bovine kidney, N-acetyl-O-desulfated heparin, and dextran were obtained from Sigma-Aldrich (St. Louis, MO). Disodium 1,3-propanedisulfonate (eprodisate) was purchased from Alfa Aesar (Pelham, NH), and homotaurine (tramiprosate) was obtained from Toronto Research Chemicals (North York, Ontario, Canada).

Aggregation Kinetics Measured by Thioflavin T Fluorescence. Reactions were conducted as above-mentioned, except that ThT (from a 1 mM stock solution) was added to reach a final concentration of 20 μM. ThT fluorescence was measured every 5 min (unless otherwise specified) over the course of 30 h, using a Gemini SpectraMax EM fluorescence plate reader (Molecular Devices, Sunnyvale, CA). The fluorescence, with excitation at 440 nm and emission at 485 nm, was measured from the bottom of the well. For each experiment, control reactions (without TTR) were carried out. The data obtained from triplicate wells were averaged, corrected by subtracting the corresponding control reaction, and plotted as fluorescence vs time. Each curve represents the average of at least three independent experiments performed in triplicate.

Circular Dichroism Spectroscopy. M-TTR (300 μL of 0.4 mg/mL in buffer A) was mixed with an equivalent volume of 200 mM acetate buffer (pH 4.8), and 3 μL of heparin (4 mg/mL diluted in water) or water was added. After the desired incubation time at 37 °C without stirring, the aggregation reaction sample was incorporated into a 2 mm path length Suprasil quartz cell. Far-UV CD spectra of the aggregated samples were recorded from 205 to 260 nm using an AVIV 202SF CD spectrometer (AVIV, Lakewood, NJ) equipped with a Peltier thermostated cell holder. The wavelength step was set at 1 nm with an average time of 30 s per scan at each wavelength step, and the temperature was set at 25 °C. Each spectrum represents the average of at least two independent experiments. For kinetic experiments, 300 μL of a 2× solution of M-TTR (0.6, 0.5, 0.4, 0.3, and 0.2 mg/mL) in buffer A was mixed with an equivalent volume of 200 mM acetate buffer (pH 4.8), and 3 μL of heparin (4 mg/mL diluted in water) or water was added. The reaction mixture was immediately incorporated into a 2 mm path length Suprasil quartz cell, and the ellipticity at 218 nm (θ_{218nm}) was measured every 5 s over the course of 60 min at 37 °C. The dead time of this experiment, before the first data can be recorded, is estimated at 20 s. Each spectrum represents the average of two independent experiments. Plots of θ_{218nm} vs time were analyzed with a procedure of best fit for the individual apparent first and second phase of structural transition using the single exponential function:

$$\theta_t = A_x e(-k_x t) + \theta_{plateau}$$

Size Exclusion Chromatography. M-TTR (200 μL of 0.4 mg/mL in buffer A) was mixed with an equivalent volume of 200 mM acetate buffer (pH 4.8), and 2 μL of heparin (4 mg/mL diluted in water) or water was added. After the desired incubation time at 37 °C without stirring, samples were filtered through a 0.22 μm PVDF membrane filter, and 200 μL was injected on a calibrated Superdex 75 HR 10/30 gel filtration column (Amersham Biosciences, Piscataway, NJ). The mobile phase was buffer A. Eluates were analyzed by UV detection at 280 nm, and the peaks corresponding to M-TTR (elution volume of 11.6−13.2 mL) or soluble aggregates (> 100 kDa) (void volume; 7−9.5 mL) were integrated and plotted as peak area vs time of aggregation. After filtration, the filters were washed with 500 μL of 8 M guanidinium chloride (GdnCl), and the total amount of M-TTR (filtered aggregates) was estimated using UV absorbance at 280 nm and expressed as a percentage of protein recovery.

Dynamic and Static Light Scattering. M-TTR (2.5 mL of 0.4 mg/mL in buffer A) was mixed with an equivalent volume of 200 mM acetate buffer (pH 4.8), and 25 μL of heparin (4 mg/mL diluted in water) or water was added. The reaction mixture was incorporated into a 20 mL disposable scintillation vial and loaded into a Dawn EOS light scattering photometer (Wyatt Tehcnology, Santa Barbara, CA). The temperature of the sample cell was set at 37 °C. Multiangle light scattering intensity and dynamic light scattering of M-TTR sample aggregation samples were recorded every 2 s over the course of 120 min at 37 °C. The hydrodynamic radius (R_h) of the samples was calculated using the Astra software package from Wyatt Technology.

Fluorescence Anisotropy. Fluorescein-labeled heparin was prepared according to the procedure reported by Glabe et al. (*59*). Briefly, the reducing end of heparin was activated by CNBr in water, pH 11, for 10 min at room temperature. The excess of CNBr was then removed by running the reaction mixture over a G-25 desalting column. The mobile phase was 0.2 M sodium borate, pH 8.0. The eluate was then mixed with fluoresceinamine. After overnight incubation at room temperature, the unreacted fluoresceinamine was removed using a G-25 desalting column. The mobile phase was 50 mM sodium phosphate, 100 mM NaCl, and 0.02% NaN_3, pH 6.8. For the assay, 500 μL of TTR variants (M-TTR, T119M TTR and V30M M-TTR) at 0.4 mg/mL in buffer A was mixed with an equivalent volume of 200 mM acetate buffer (pH 4.8 or pH 5.2). Fluorescein-labeled heparin (6.7 μL of a 3 mg/mL stock solution) was added to the aggregation mixture, to reach a final concentration of 20 μg/mL. Samples were incubated at 37 °C, and at specific time points, a 100 μL aliquot was taken, and the fluorescence polarization was measured using an AVIV ATF-105 spectrofluorometer (AVIV, Lakewood, NJ). The excitation was set at 490 nm (2 nm bandwidth) and the emission at 514 nm (2 nm bandwidth). Each reading was taken five times, and final data represent at least three independent experiments. For some experiments, purified TTR of different aggregation states at a concentration of 0.4 mg/mL in buffer A was mixed with an equivalent volume of 10 mM phosphate buffer (pH 7.6) or 200 mM

acetate buffer (pH 4.8), and fluorescence polarization was immediately measured as described above.

Preparation and Purification of TTR of Various Aggregation States. M-TTR insoluble aggregates, including amyloid fibrils, were obtained by incubating TTR under acidic conditions. M-TTR at a concentration of 0.4 mg/mL in buffer A was mixed with an equivalent volume of 200 mM acetate buffer (pH 4.8). Samples were incubated for 5 days at 37 °C, and the fibrils were recovered by centrifugation at 13000*g* for 30 min at room temperature. The fibrils were washed once with buffer A before being finally resuspended in buffer A. The aggregates were judged to be fibrils by ThT fluorescence. Large soluble aggregates were obtained as previously described (*10*). Briefly, a 6 mg/mL M-TTR in Opti-MEM (Invitrogen, Grand Island, NY) solution was filter sterilized and incubated at 37 °C for 5 days. After incubation, M-TTR solution was filtered through a 0.22 μm filter and purified on a Superdex 75 gel filtration column in buffer A. The peak eluting in the void volume of the column which corresponds to large soluble aggregates (100−10000 kDa) (*10*) was collected. M-TTR and V30M M-TTR oligomers were obtained by incubating a 6 mg/mL solution in Opti-MEM for 5 days at 4 °C. After incubation, protein solutions were filtered through a 0.22 μm filter and purified on a Superdex 75 gel filtration column in buffer A. The peak corresponding to oligomers (estimated sizes of 25−90 kDa (*10*)) was collected.

8-Anilinonaphthalene-1-sulfonate Fluorescence. M-TTR insoluble aggregates prepared in the absence or presence of 20 μg/mL heparin and isolated as described above were resuspended in buffer A. Aliquots of 8-anilinonaphthalene-1-sulfonate (ANS) in buffer A were added to the aggregates or to monomeric M-TTR solution to reach a final ANS concentration ranging from 0 to 400 μM. The final protein concentration was 0.2 mg/mL. The fluorescence spectra were immediately recorded using a Varian Cary Eclipse spectrofluorometer (Varian, Santa Clara, CA). The excitation was set at 380 nm, and fluorescence emission was acquired between 450 and 500 nm. Each spectrum was taken twice and blank-subtracted (corresponding ANS concentration, without protein). The fluorescence intensity at 470 nm measured without ANS (only 0.2 mg/mL protein) was finally subtracted from the blank-subtracted fluorescence.

Limited Proteolysis Experiments. M-TTR aggregates grown for 5 days at 37 °C in the presence or absence of 20 μg/mL heparin were isolated by centrifugation, washed twice with buffer A, and resuspended in 50 mM Tris-HCl buffer, pH 8.0. Aggregates were then incubated with trypsin using an enzyme-to-substrate ratio of 1:200 (w/w) at 37 °C or with proteinase K (PK) at a ratio of 1:2000 (w/w) at 25 °C. After the desired digestion times, samples were analyzed by SDS−PAGE and the bands detected by Coomassie blue staining were quantified using an Odyssey Li-COR imager (Lincoln, NE). After solubilization of the digested aggregates in 8 M GdnCl, samples were also subjected to liquid chromatography coupled ESI mass spectrometry analysis using an Agilent 1100 MSD LC/MS quadrupole mass spectrometer (Santa Clara, CA).

RESULTS

Effect of GAGs on TTR Aggregation. The influence of various GAGs on TTR amyloidogenesis was monitored by ThT binding (*60*) and by turbidity at 400 nm (*53*) under quiescent conditions. TTR amyloidogenesis was mediated in the present study by partial acid denaturation (*47*, *48*) because the stability of the TTR tetramer at neutral pH makes TTR amyloidogenesis very inefficient, except for the most destabilized TTR variants. Among the GAGs studied, heparin was most effective at promoting WT TTR aggregation, as revealed by the increased slopes of the aggregation reaction and the higher ThT fluorescence and turbidity measurements (Figure 1A, red traces). Heparin is a highly sulfated GAG, having an average of 1.6−3 sulfate groups per disaccharide repeat unit (Figure 1B). Dermatan sulfate (chondroitin B), chondroitin A, chondroitin C, and keratan sulfate, less sulfated GAGs (*61*), also promoted the aggregation of WT TTR, although these were less effective compared to heparin (Figure 1A and Supporting Information Figure S1A). In contrast, hyaluronic acid, a nonsulfated GAG, had no significant effect on WT TTR aggregation kinetics.

Very similar GAG acceleration results were obtained using the engineered monomeric version of TTR (M-TTR) (Figure 1C and Supporting Information Figure S1B). Introduction of the F87M and L110M mutations into the dimer−dimer interfaces of TTR prevents its tetramerization by steric hindrance, without affecting M-TTR tertiary structure (*52*). Although M-TTR and WT TTR show similar tertiary structural stabilities, M-TTR aggregates 100-fold faster than WT TTR (*52*, *55*), because tetramer dissociation, normally rate limiting for aggregation, is not required for M-TTR aggregation (*47*, *48*). The present data also show that M-TTR exhibited a higher rate of aggregation at pH 4.8 compared to WT TTR, as measured by both ThT fluorescence and turbidity (cf. Figure 1A,C; note the *y* and *x* axis differences). M-TTR aggregation reactions recorded by turbidity at 400 nm (carried out without stirring) are truncated at 5 h, as large aggregates start to sediment afterward, interfering with turbidity measurements (Figure 1C, right panel). Taken together, these results indicate that GAGs induce M-TTR and WT TTR aggregation, and the propensity to do so correlates with their degree of sulfation.

The stimulating effect of heparin on pH-induced M-TTR aggregation was concentration dependent over the range of 1−20 μg/mL, before reaching a plateau at concentrations above 20 μg/mL, according to ThT fluorescence and turbidity measurements (Figure 1D). Therefore, a molar ratio of approximately 1 heparin chain (20 μg/mL; assuming an average molecular mass of 15 ± 2 kDa) per 10 TTR monomers (0.2 mg/mL) appears to be optimal for accelerating M-TTR aggregation. This is consistent with a computational approach supported by experimental data suggesting that the GAG effect on protein aggregation is maximal at a 1:10 molar ratio, respectively (*62*).

Importance of Heparin Sulfation and High Molecular Weight for Accelerating M-TTR Amyloidogenesis. The significance of sulfate functional groups on GAGs for accelerating amyloidogenesis has been reported previously for gelsolin (*25*), Aβ (*27*), and IAPP (*63*). To further explore the role of the sulfate groups for inducing TTR aggregation, heparin analogues with various sulfate substitutions were employed (Figure 1B). The sparingly sulfated heparin derivative, HS, exhibiting an average of 0.4−2 sulfate groups per disaccharide (*61*) slightly induced M-TTR aggregation (Figure 2A, green trace). Similarly, *N*-acetylheparin (Figure 2A, blue trace) with two potential sites of sulfation per disaccharide (Figure 1B; R_2 = acetyl) was less efficient at inducing TTR aggregation than heparin ($R_2 = SO_3^-$, Figure 2A, red trace), highlighting the crucial role of the sulfate groups. We also tested the capacity of heparin chains of various lengths to influence M-TTR amyloid formation. An eight monosaccharide unit (dp8), composed of

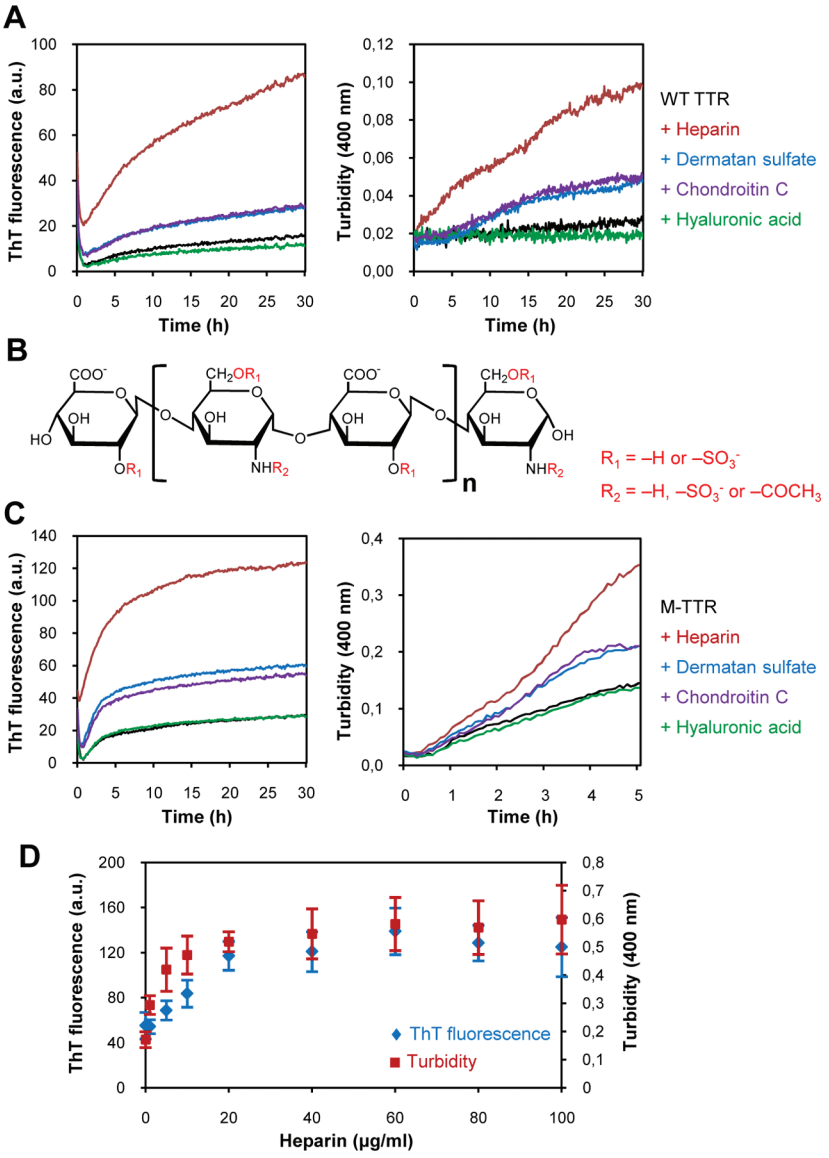

FIGURE 1: Influence of glycosaminoglycans on WT TTR and M-TTR aggregation kinetics. (A) WT TTR aggregation was assessed by the increase of ThT fluorescence (left panel) or the increase in turbidity at 400 nm (right panel). WT TTR (0.2 mg/mL) was incubated in 200 mM acetate buffer, pH 4.8, 37 °C, in the absence (black) or in the presence of 20 μg/mL heparin (red), dermatan sulfate (blue), chondroitin C (purple), or hyaluronic acid (green). (B) Representative structure of heparin composed of glucuronic acid (GlcA) linked to glucosamine (GlcN) disaccharide repeating subunit. R_1 could be $-H$ or $-SO_3^-$ whereas R_2 could be $-H$, $-SO_3^-$, or $-COCH_3$. (C) M-TTR aggregation assessed by ThT fluorescence and turbidity at 400 nm using the same conditions as in (A) and presented analogously. (D) M-TTR (0.2 mg/mL) was incubated in 200 mM acetate buffer, pH 4.8, 37 °C, for 30 h in the presence of increasing heparin concentrations (1−100 μg/mL), and the aggregation was assessed by ThT fluorescence (blue diamonds) and turbidity at 400 nm (red squares) at the end of the 30 h incubation period. For turbidity readings, samples were agitated for 5 s before the reading.

(IdoA,2S−GlcNs,6S), was the shortest oligomer tested that accelerated M-TTR aggregation (Figure 2B, blue trace). Heparin fragments composed of two or four monosaccharides did not significantly stimulate M-TTR amyloidogenesis (Figure 2B, orange and purple traces). In addition, low molecular mass heparin, from 3 to 7 kDa (9−21 monosaccharide units), was significantly less efficient in promoting M-TTR aggregation than high molecular mass heparin varying from 13 to 17 kDa (40−52 monosaccharide units) (Figure 2B). This is in contrast to observations made with gelsolin and Aβ, intrinsically disordered polypeptides, where four monosaccharide units (*25*) and chondroitin sulfate-derived disaccharides (*64*), respectively, were sufficient to induce amyloidogenesis. Taken together, our results indicate that a high density of sulfate groups and the polymeric nature of GAGs are essential features for accelerating TTR aggregation.

Influence of Ionic Strength and GAG Mimetics on Heparin-Accelerated M-TTR Aggregation. To probe the hypothesis that the influence of GAGs on amyloidogenesis is governed by electrostatic interactions (*28*, *65*), we recorded M-TTR aggregation time courses as a function of salt concentration. The addition of NaCl (100 or 250 mM) reduced the amyloid-promoting effect of heparin on M-TTR amyloidogenesis, suggesting that high salt concentrations can shield heparin−TTR electrostatic interactions (Figure 3A). We next investigated the effect of sulfated GAG mimetics, such as propane-1,3-disulfonate (eprodisate) (*66*) and homotaurine (tramiprosate) (*67*), that have been postulated to inhibit the formation of amyloid by interfering with the amyloidogenic protein−GAG interaction. Addition of disodium propane-1,3-disulfonate (0.72 mM) or homotaurine (0.49 mM) to an M-TTR aggregation

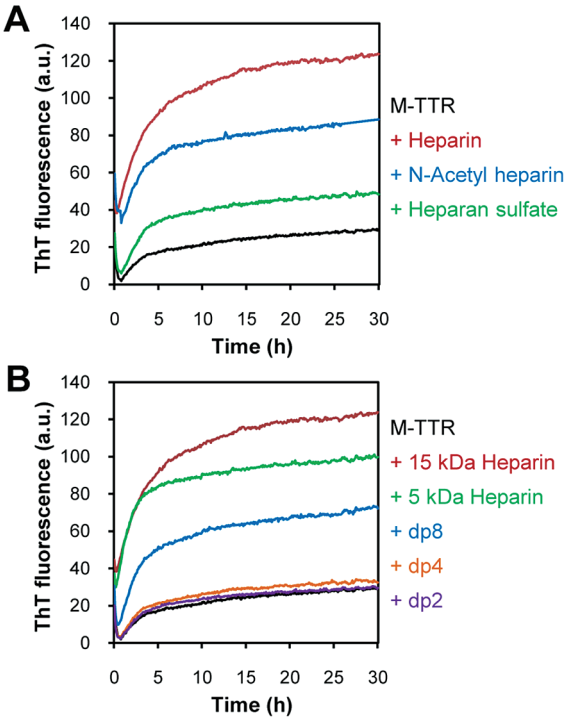

FIGURE 2: Effects of heparin sulfation state and molecular weight on heparin-accelerated M-TTR aggregation. (A) M-TTR (0.2 mg/mL) was incubated in 200 mM acetate buffer, pH 4.8, 37 °C, in the absence (black) or in the presence of 20 μg/mL heparin (red), *N*-acetylheparin (blue), or heparan sulfate (green). (B) M-TTR (0.2 mg/mL) was incubated in 200 mM acetate buffer, pH 4.8, 37 °C, in the absence (black) or in the presence of 20 μg/mL 15 kDa heparin (red), 5 kDa heparin (green), eight saccharide unit heparin (dp8, blue), four saccharide unit heparin (dp4, orange), or UA,2S−GlcNS,6S disaccharide (dp2, purple).

assay did not reduce the accelerating effect of heparin on M-TTR amyloidogenesis (Figure 3B), consistent with the data in Figure 2B showing that at least an eight monosaccharide unit GAG is required to affect amyloidogenesis. Moreover, neither homotaurine nor propane-1,3-disulfonate alone significantly influenced pH-mediated TTR aggregation (Figure 3B), consistent with their inability to make multivalent interactions. These results suggest that it is unlikely that GAG mimetics can slow down TTR amyloidogenesis by inhibiting the interaction between amyloidogenic proteins and GAGs.

Effect of Heparin Addition to an Ongoing TTR Aggregation Reaction. We next investigated the effect of introducing heparin after a pH-mediated M-TTR aggregation reaction (pH 4.8, 37 °C) had begun. Addition of heparin into an ongoing aggregation reaction at times indicated by the arrows (Figure 3C) led to a very rapid increase in ThT fluorescence. This phenomenon could be ascribed to several, not necessarily exclusive, mechanisms. Heparin could affect the morphology and/or the degree of rigidity of the preformed aggregates, leading to an increase in ThT binding, or it could increase the quantity of fibrils and/or β-sheet-rich aggregates formed by interacting with the remaining ThT-negative soluble oligomers in solution. Alternatively, heparin addition could influence the preaggregate portion of the amyloid cascade, namely, by shifting the folded monomer−amyloidogenic monomer equilibrium to the right, or the like.

To investigate if the observed ThT increases upon heparin addition in Figure 3C correspond to the formation of new aggregates, we performed an analogous aggregation reaction without

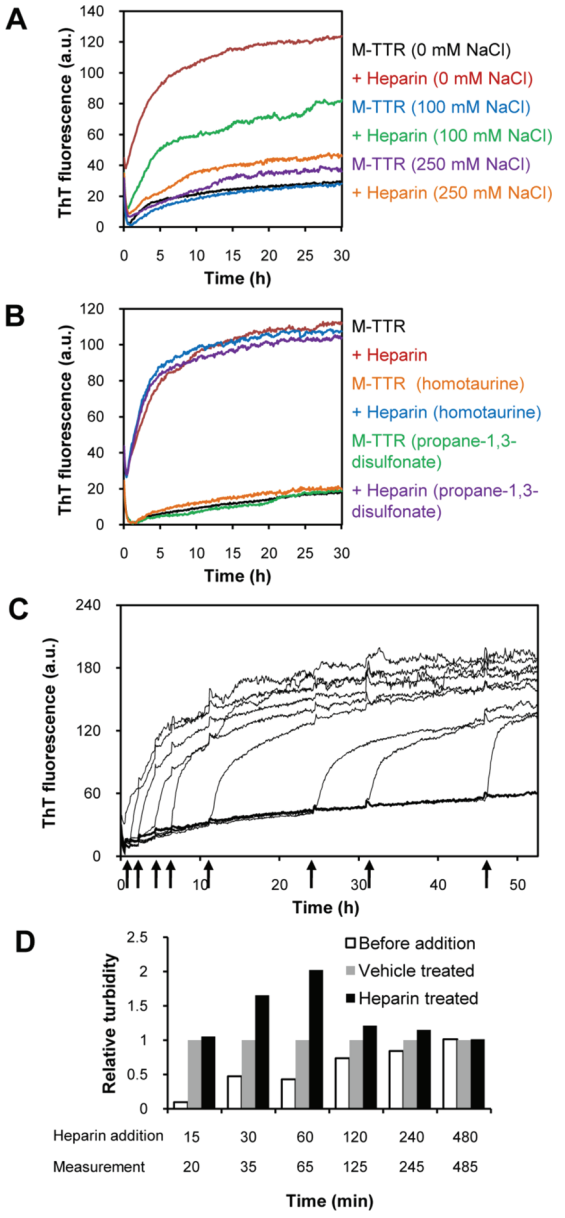

FIGURE 3: Effect of salt concentration, glycosaminoglycan mimetics, and time of heparin addition on heparin-accelerated M-TTR aggregation. (A) M-TTR (0.2 mg/mL) was incubated in 200 mM acetate buffer, pH 4.8, 37 °C, in the absence (black, blue, purple) or in the presence of 20 μg/mL heparin (red, green, orange). NaCl concentration was adjusted to 250 mM (orange, purple), 100 mM (green, blue), or 0 mM (red, black), respectively. (B) M-TTR (0.2 mg/mL) was incubated in 200 mM acetate buffer, pH 4.8, 37 °C, in the absence (black, red) or in the presence of 100 μg/mL homotaurine (blue, orange) or 100 μg/mL propane-1,3-disulfonate (purple, green). Heparin, at a concentration of 20 μg/mL, was added (red, blue, purple) or not (black, green, orange). (C) M-TTR (0.2 mg/mL) was incubated in 200 mM acetate buffer, pH 4.8, 37 °C, and 20 μg/mL heparin was added at different times after the start of the M-TTR aggregation, indicated by the arrows. (D) M-TTR (0.2 mg/mL) was incubated in 200 mM acetate buffer, pH 4.8, 37 °C. At different times (15, 30, 60, 120, 240, and 480 min; *x* axis), after the start of M-TTR aggregation, 20 μg/mL heparin or water (vehicle) was added. Immediately before the heparin or vehicle addition, samples were gently vortexed, and optical density was measured (white bars, before addition). After heparin or vehicle addition, quiescent incubation at 37 °C was resumed for an additional 5 min, and then turbidity was measured after mild vortexing (vehicle-treated samples are depicted by gray bars, whereas heparin-treated samples are represented by black bars). The relative turbidity in M-TTR samples without heparin addition (vehicle treated, gray bars) was assigned to be unity.

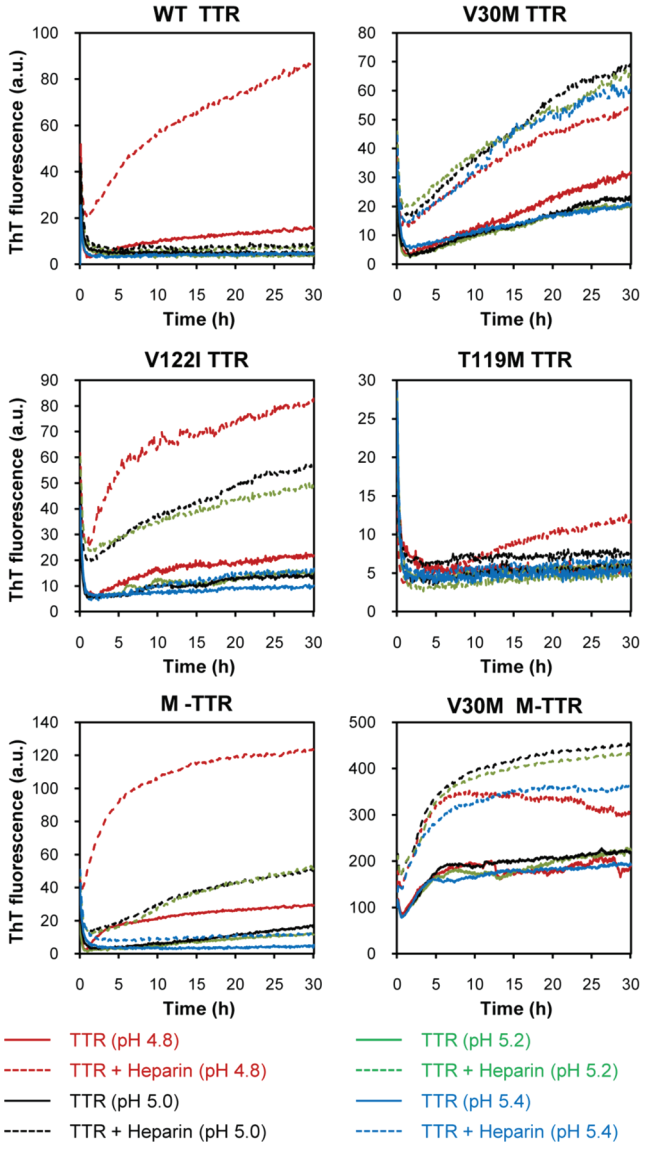

FIGURE 4: Influence of TTR kinetic and/or thermodynamic stability on heparin-accelerated aggregation. TTR (0.2 mg/mL) variants were incubated in 200 mM acetate buffer, 37 °C, in the absence (solid line) or presence (dashed line) of 20 μg/mL heparin. The pH was adjusted to 4.8 (red), 5.0 (black), 5.2 (green), or 5.4 (blue).

adding heparin. After 30 h (where heparin-accelerated amyloidogenesis is maximal), the contents of triplicate wells were isolated by centrifugation (30 min, 13000*g*), and the concentrations of M-TTR in the supernatant and the pellet were determined by measuring absorbance at 280 nm (each at 8 M GdnCl to disassemble the aggregates). No M-TTR was detectable in the supernatant at 30 h, whereas most of the protein (86% of the initial protein content) was recovered in the pellet. Analogous time-dependent experiments reveal that aggregation of M-TTR (pH 4.8, 37 °C) is, in fact, complete between 5 and 6 h in the absence of heparin. These results suggest that the sharp increase in ThT fluorescence observed after heparin addition to an ongoing aggregation reaction (Figure 3C) is unlikely the result of forming a larger quantity of insoluble aggregates, as the M-TTR molecules have already aggregated. Therefore, heparin is more likely affecting aggregate morphology by templating preformed aggregates to convert to larger and/or better defined aggregates by quaternary structural conversion.

The influence of adding heparin later in the time course of M-TTR aggregation (pH 4.8, 37 °C) was also investigated by assessing turbidity, in contrast to the ThT fluorescence data in Figure 3C. The addition of heparin 15 min after the beginning of an acid-mediated M-TTR aggregation reaction (Figure 3D, 15 min) did not increase the turbidity measured at 20 min relative to the sample without heparin added (Figure 3D, 20 min). However, addition of heparin later into the time course of the M-TTR aggregation (Figure 3D, 30, 60, 120, and 240 min) led to an increase in turbidity assessed 5 min after heparin addition, as compared to vehicle control (Figure 3D). These results are consistent with the ThT fluorescence results (Figure 3C) suggesting that heparin is most likely acting by accelerating the conversion of preformed oligomeric structures into larger aggregates. Turbidity is related to both the amount and size of the aggregates formed (*53*), whereas ThT fluorescence is proportional to the extent of cross-β-sheet structure (*60*), the former being less sensitive at the early and late stages of aggregation.

Effect of Heparin on TTR Amyloidogenesis as a Function of TTR Stability. In order to obtain insights into the mechanism(s) by which heparin accelerates TTR amyloidogenesis, we investigated the effect of heparin on the aggregation of well-characterized TTR variants. These include the amyloid disease-associated variants V30M, V122I, and A25T (*55*), which form destabilized homotetramers, the kinetically stable variant T119M, which forms a tetramer with an increased tetramer dissociation barrier as a result of transition state destabilization (*68*), and the unstable V30M monomeric variant (V30M M-TTR) (*56*). The WT TTR tetramer does not dissociate at pH > 5.0, and heparin did not significantly stimulate its amyloidogenesis at pH > 5.0 (Figure 4).

In contrast, V30M TTR aggregation kinetics were affected by heparin over a broader pH range, consistent with the established ability of the V30M TTR tetramer to dissociate into amyloidogenic monomers at pHs ranging from 4.8 to 5.4 (Figure 4) (*69*). The pH-dependent aggregation of the V122I TTR homotetramer was very similar to that observed for M-TTR, with heparin accelerating amyloidogenesis over the pH range of 4.8−5.2, consistent with the thermodynamic and kinetic instability of the V122I tetramer over this pH range (*6*, *52*, *55*, *70*). As expected, T119M amyloidogenesis is only slightly accelerated by heparin at pH 4.8 (Figure 4), owing to the increased kinetic stability of the T119M TTR tetramer rendering it less susceptible to dissociation (*6*, *51*, *68*). Finally, V30M M-TTR, which is known to have an unstable tertiary structure (*55*), and the A25T TTR, established to have an unstable tetrameric structure (*55*), both exhibited a strong increase of ThT fluorescence upon incubation in acetate buffer over the pH range of 4.8−5.4, and in all cases heparin accelerated their amyloidogenesis (Figure 4 and Supporting Information Figure S2, respectively). Notably, in all cases, heparin acceleration of amyloidogenesis is only observed if aggregation was already occurring at that pH in the absence of heparin, suggesting that heparin can accelerate TTR amyloidogenesis either by interacting with partially denatured TTR species and/or with aberrant assemblies of TTR.

Taken together, these results strongly suggest that heparin does not significantly influence TTR tetramer stability or TTR dissociation kinetics. Instead, the presence of heparin seems to facilitate partially unfolded TTR to misassemble with higher efficiency and/or increase the rate of conversion of TTR oligomers into ThT positive aggregates. It is notable that none of the above-mentioned variants, including the unstable V30M M-TTR

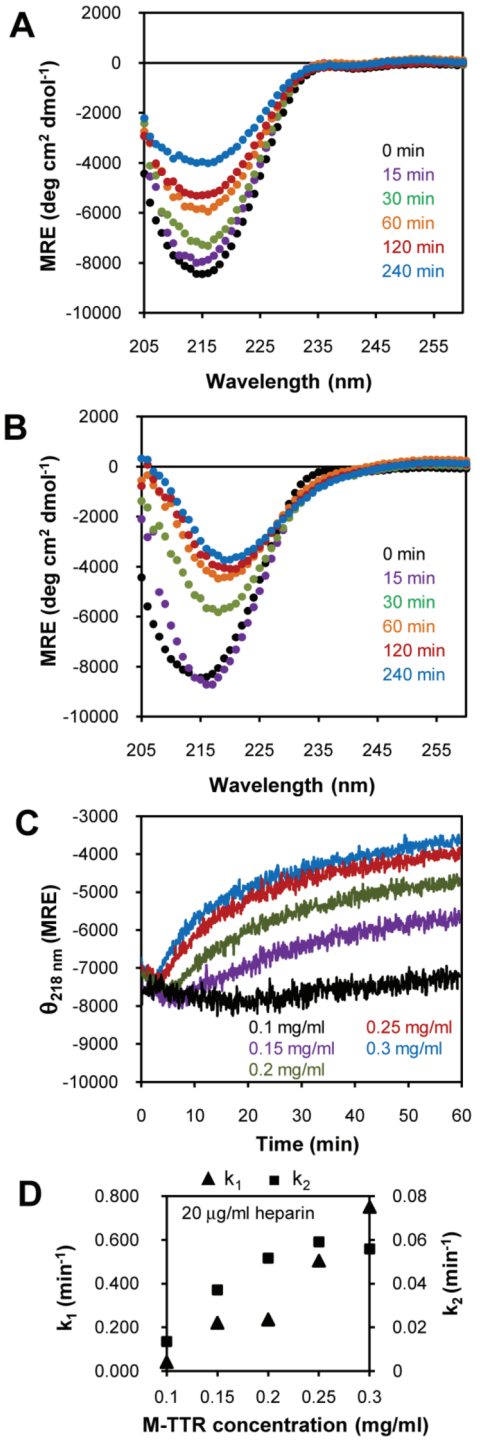

FIGURE 5: Effect of heparin on acid-induced M-TTR tertiary and/or quaternary structural changes. (A, B) Far-UV CD spectra of 0.2 mg/mL M-TTR samples aggregated without (A) or with 20 μg/mL heparin (B) in 200 mM acetate buffer, pH 4.8, 37 °C. Spectra were read at 0 (black), 15 (purple), 30 (green), 60 (orange), 120 (red), and 240 min (blue) after the beginning of the acid-mediated aggregation process. Time 0 min (black) corresponds to a pH 7.6 control. (C) M-TTR was incubated in 200 mM acetate buffer, pH 4.8, at 37 °C in the presence of 20 μg/mL heparin at a M-TTR concentration of 0.3 (blue), 0.25 (red), 0.2 (green), 0.15 (purple), or 0.1 mg/mL (orange). (D) Dependence of M-TTR conformational change rates on M-TTR concentration in the presence of 20 μg/mL heparin. The change in the β-sheet signal measured at 218 nm, reported in (C), was analyzed using a best fit procedure. k_1 (▲) and k_2 (■) are first-order rate constants of the apparent first and second phase of the structural changes, respectively, obtained with a procedure of best fit, using the single exponential function ($\theta = A_x \exp(-k_x t) + \theta_{plateau}$).

monomer, showed a significant increase in aggregation rate in the presence of heparin early in the aggregation course at pH ≥5.6 (Supporting Information Figure S3). This was true even when amyloidogenesis was observed by ThT fluorescence in the absence of heparin (Supporting Information Figure S3). Collectively, these results suggest not only that the ability of heparin to accelerate TTR amyloidogenesis is connected to the presence of misfolded monomers and/or oligomers, but that these TTR species must be positively charged to interact efficiently with heparin. TTR has a theoretical isoelectric point (p*I*) of 5.48.

Effect of Heparin on M-TTR Tertiary and/or Quaternary Structural Transitions. M-TTR pH-induced tertiary and/or quaternary structural transitions were recorded by far-UV CD spectroscopy as a function of time. Incubation of M-TTR (0.2 mg/mL) at 37 °C in acetate buffer (pH 4.8) resulted in an M-TTR conversion from its native β-sheet-rich structure into a misfolded and/or misassembled state, as discerned by the progressive decrease of the β-sheet minimum at 215 nm (Figure 5A). When heparin was added to the aggregation time course, M-TTR exhibited a red shift in its minimum after 15 min, from 215 to 217 nm (Figure 5B). This spectral shift was followed by a more rapid decrease in ellipticity at 215 nm, most likely a consequence of an increase in β-sheet quaternary structure and/or the formation of cross-β-sheet amyloid fibrils. The red shift in the β-sheet minimum in the presence of heparin was notable, indicating that heparin influences the quaternary or cross-β-sheet structure of aggregating M-TTR. These results suggest that heparin accelerates the structural transition of M-TTR from its native β-sheet-rich structure to what is most likely to be an aggregated form of M-TTR.

To scrutinize whether the observed structural transition is attributable to a conformational transition involving monomeric M-TTR or rather to an aggregation event, the ellipticity of M-TTR at 218 nm (θ_{218nm}) was recorded as a function of concentration (0.1−0.3 mg/mL) in the absence or presence of heparin. The observed θ_{218nm} changes occurred faster as the concentration of M-TTR increased (Figure 5C and Supporting Information Figure S4), a telltale sign that aggregation is driving these structural transitions. Kinetic traces were then analyzed with a best fit procedure, and the apparent first (k_1) and second (k_2) phases were analyzed individually with a single exponential function. As observed in Figure 5D and Supporting Information Figure S4, both k_1 and k_2 values featured a clear dependence on M-TTR concentration, indicating that the observed changes of θ_{218nm} were associated with aggregation at a concentration above 0.1 mg/mL (7.2 μM). At a concentration of 0.1 mg/mL, it is clear that heparin does not considerably alter the folded monomer−misfolded monomer equilibrium in the absence of aggregation. Collectively, these data demonstrate that aggregation is the driving force for the β-sheet quaternary structural change observed at concentrations above 0.15 mg/mL and that aggregation is required for heparin to have an accelerating effect. Thus, evidence is mounting for the hypothesis that aggregates must be present for heparin to accelerate TTR aggregation.

Effect of Heparin on M-TTR Aggregation Monitored by Size Exclusion Chromatography. The acid-mediated aggregation of M-TTR as a function of time was monitored by injecting filtered (0.22 μm, PVDF membrane filter) aliquots onto a Superdex 75 HR size exclusion column. The monomer peak, eluting at 12.2 mL, decreased gradually over time in the absence of heparin (Figure 6A). In contrast, the peak corresponding to large soluble aggregates (> 100 kDa), eluting in the void volume (7−9 mL), showed a sharp increase after 30 min, was maximal at

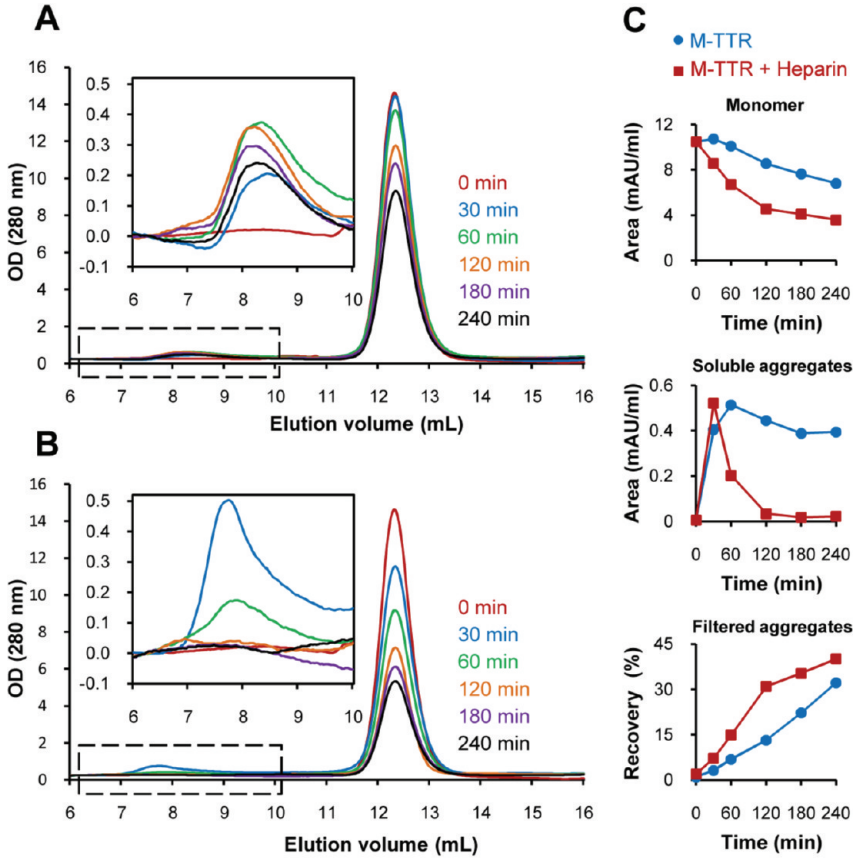

FIGURE 6: Influence of heparin on M-TTR aggregation monitored by analytical gel filtration chromatography. (A, B) Chromatograms of M-TTR (0.2 mg/mL) at pH 4.8, 37 °C, in the absence of heparin (A) or in the presence of 20 μg/mL heparin (B) obtained after 0 (red), 30 (blue), 60 (green), 120 (orange), 180 (purple), and 240 min (black). The insets show the same data with an expanded OD scale to emphasize the differences in the peak area corresponding to the soluble aggregates. (C) Integration of monomer and soluble aggregates (void volume) peaks as well as the aggregates retained by the 0.22 μm PVDF membrane filter (expressed as protein recovery (%)) reported as a function of time into the aggregation reaction performed in the absence (●) or in the presence of 20 μg/mL heparin (■).

60 min, and then steadily decreased, most likely because the precolumn filter removed macroscopic aggregates. In the presence of heparin, the monomer peak decreased much more rapidly as a function of time, while large soluble aggregates appeared at 30 min and disappeared after 120 min (Figure 6B), again most likely as a consequence of filter retention. To confirm the assumption that larger aggregates are retained by the 0.22 μm PVDF membrane, the filters were washed with a solution of 8 M GdnCl, and the M-TTR concentration of the filtrate was measured. More M-TTR is retained by the filter when the aggregation reaction was performed in the presence of heparin (Figure 6C, bottom panel). Integration of the soluble aggregates and monomer peak areas (Figure 6C) confirm that heparin accelerates the initial conversion of monomeric M-TTR into soluble aggregates, which elute in the void volume, and promotes their association into larger aggregates that are retained by the filter. The more rapid disappearance of monomeric M-TTR in the presence of heparin likely reflects the fact that the monomer−misfolded amyloidogenic monomer−oligomer−TTR fibril equilibria are all linked. Thus, heparin-induced acceleration of the oligomer to TTR fibril rate will also shift the other equilibria by Le Chatelier's principle. Nonetheless, we cannot totally exclude the possibility that heparin can also accelerate TTR aggregation by converting monomeric TTR into oligomers, although the data that heparin does not accelerate the early phase of the M-TTR aggregation, as measured by turbidity (Figures 1C and 3D), are not consistent with this possibility.

Effect of Heparin on M-TTR Aggregation Monitored by Static and Dynamic Light Scattering. In order to further understand the influence of heparin on aggregate size during acid-mediated M-TTR aggregation, static and dynamic light scattering experiments were employed. The light scattering intensity at 90° increased during acid-mediated M-TTR aggregation (Figure 7A). In the absence of heparin, the light scattering intensity increased sharply between 20 and 60 min and then stabilized (Figure 7A, black trace). To probe whether the apparent plateau is due to a decrease in the concentration of particles in solution through sedimentation during the quiescent time course, the sample was vortexed after 120 min, and light scattering monitoring was resumed. The light scattering intensity did not increase significantly and remained constant over time, suggesting that the apparent plateau is not related to sedimentation (data not shown). Since the total mass used for the aggregation reaction is constant over the time course of aggregation, the increased intensity of scattered light at 90° is related to the increase in the size of the aggregates. When heparin was added to the aggregation reaction, the initial increase of the light scattering intensity in the time course (up to 50 min) did not change (Figure 7A, cf. red trace with heparin to black trace without), consistent with the data interpretation above: that heparin does not accelerate tetramer dissociation or shift the monomer−misfolded monomer equilibrium directly, nor does heparin influence the early phase of M-TTR aggregation as measured by turbidity (Figures 1C and 3D). However, in the presence of

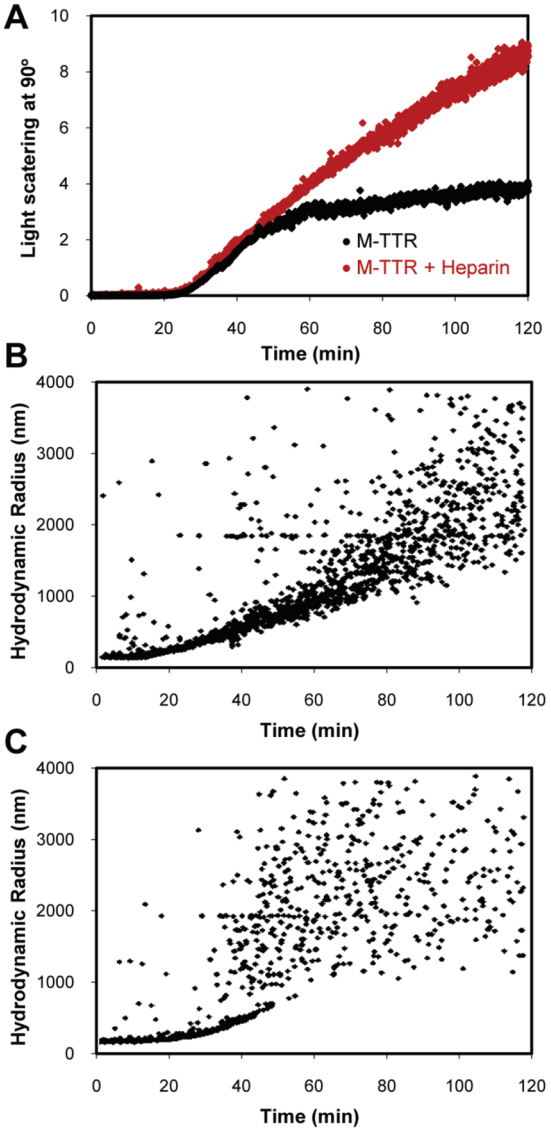

FIGURE 7: Effect of heparin on M-TTR aggregation monitored by dynamic light scattering. (A) M-TTR (0.2 mg/mL) was incubated in 200 mM acetate buffer, pH 4.8, 37 °C, in the absence (black) or presence (red) of 20 μg/mL heparin. The light scattering intensity at 90° was measured every 2 s. (B, C) Hydrodynamic radius (R_h) assessment of M-TTR aggregation as a function of time performed in the absence (B) or presence (C) of heparin. R_h was calculated using the Astra software package from Wyatt Technology.

heparin, the intensity of light scattering did not plateau after 60 min of quiescent incubation but continued to increase (Figure 7A, red trace), consistent with a quaternary structural conversion of smaller aggregates into larger aggregates that remain soluble. The hydrodynamic diameter, or Stokes radius (R_h), over the time course of aggregation was calculated using the Astra software and graphed as a function of time (Figure 7B,C). Heparin accelerated the formation of large soluble aggregates that exhibit a heterogeneous R_h > 500 nm (Figure 7C), consistent with the analytical size exclusion chromatography analysis (Figure 6) and light scattering intensity kinetics (Figure 7A). The near-exponential formation of large M-TTR aggregates in the presence of heparin (Figure 7C) contrasts with the data in the absence of heparin, exhibiting a linear more homogeneous increase of R_h over time (Figure 7B). These results strongly suggest that heparin accelerates the conversion of preformed TTR aggregates into larger aggregates by quaternary structural conversion.

Interaction of Heparin with TTR Measured by Fluorescence Anisotropy. We used fluorescence anisotropy to investigate the interactions between the various aggregation states of TTR and heparin. The polarization change was analyzed by incubating fluorescein-labeled heparin with monomeric M-TTR, tetrameric WT TTR, purified oligomers, isolated large soluble aggregates, or insoluble aggregates, at pH 4.8 and 7.6 (see Experimental Procedures for the preparation of the TTR aggregate species). Incubation of fluoresceinated heparin with native M-TTR or WT TTR (tetramer) showed no evidence for binding at either pH 4.8 or pH 7.6 (Figure 8A), consistent with results outlined above suggesting that heparin does not directly influence the beginning of the TTR amyloidogenesis cascade. At pH 7.6, the polarization of fluoresceinated heparin did not change upon incubation with large soluble aggregates or amyloid fibrils but did increase significantly upon addition of purified oligomers formed from either M-TTR or V30M M-TTR (Figure 8A), suggesting that fluoresceinated heparin can bind to oligomers. At pH 4.8, a strong increase in fluoresceinated heparin polarization was observed with all TTR aggregated species (Figure 8A), consistent with our hypothesis that heparin binds aggregates through electrostatic interactions. The interaction between fluoresceinated heparin and insoluble aggregates derived from M-TTR was further evaluated as a function of pH. The increase of polarization upon incubation with insoluble M-TTR aggregates was pH dependent (Figure 8B). Scattered light, resulting from the presence of precipitant in the sample, can lead to inaccurately high fluorescence polarization values. However, incubation of the insoluble M-TTR aggregates with fluoresceinated heparin at pH 7.6 revealed that the presence of TTR aggregates did not profoundly affect the fluorescence polarization value (Figure 8B), suggesting that the increase of polarization observed at low pH is principally related to heparin−TTR binding interactions and not to light scattering.

The kinetics of fluoresceinated heparin binding to TTR was then monitored during the acid-mediated amyloidogenesis reaction. Incubation of fluoresceinated heparin with M-TTR at pH 4.8 and pH 5.2 resulted in a gradual increase of fluorescence polarization with time (Figure 8C and Supporting Information Figure S5, respectively), over the period when aggregates appear in the absence of heparin. When the metastable V30M M-TTR variant was employed, a very sharp increase of polarization could be observed after 30 min (Figure 8C and Supporting Information Figure S5). In striking contrast, incubation of fluoresceinated heparin at pH 4.8 with the kinetically stable T119M TTR variant did not change the polarization until 24 h of incubation. By comparing these results (Figure 8C and Supporting Information Figure S5) with ThT fluorescence kinetics (Figure 4), it becomes clear that the increase of polarization tracks the formation of TTR aggregates, suggesting that heparin binds to ThT-positive TTR aggregates.

Effect of Heparin on the Structural Properties of TTR Aggregates. The accelerated increase of ThT fluorescence when heparin is added later in the time course of the M-TTR aggregation reaction (Figure 3C) suggested that heparin could affect the quaternary structure of TTR aggregates. To investigate this possibility, we compared ANS binding (*71*) and the proteolysis resistance of aggregates prepared in the absence and presence of heparin. Aggregates grown for 5 days with or without heparin showed similar levels of turbidity, whereas ThT fluorescence was higher for aggregates prepared in the presence of heparin (Figure 9A). The ANS fluorescence intensity of aggregates grown

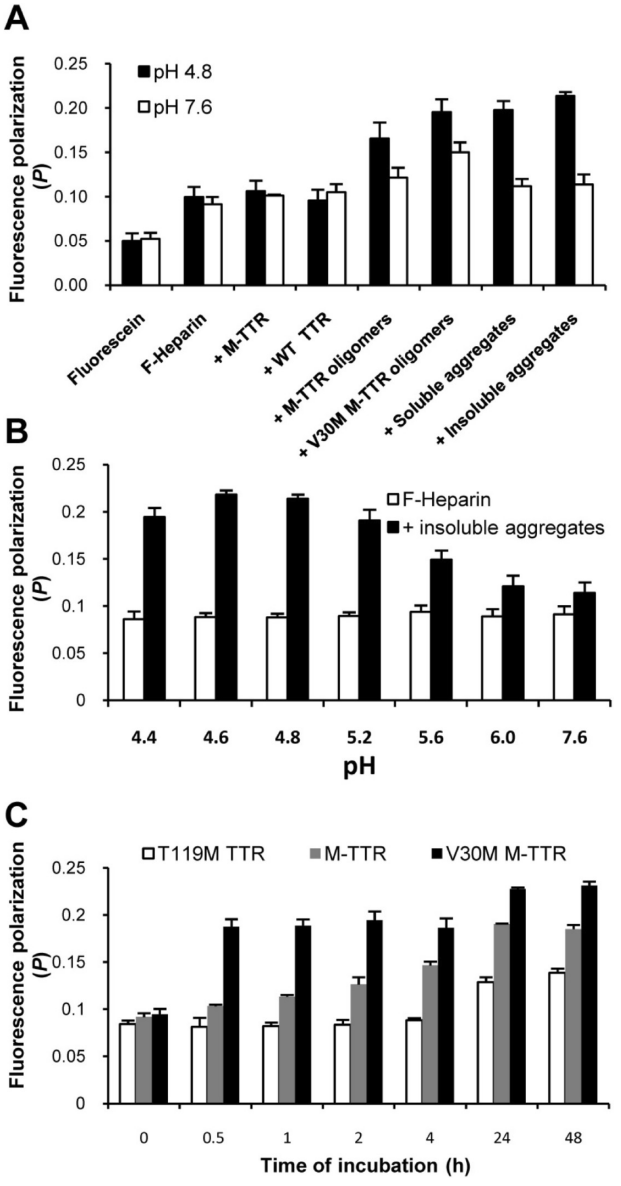

FIGURE 8: Interactions between various states of TTR and heparin assessed by fluoresceinated heparin fluorescence polarization measurements. (A) 20 μg/mL fluoresceinated heparin (F-heparin) was incorporated into a 0.2 mg/mL TTR solution (various states) at pH 7.6 (white) or the pH was adjusted to 4.8 (black) and the fluorescence polarization was immediately measured. Purified oligomers, large soluble aggregates, and fibrils were prepared as described in the Experimental Procedures section. (B) 20 μg/mL fluoresceinated heparin (F-heparin) was mixed with 0.2 mg/mL TTR fibrils (black) or not (white) as a function of pH, and the fluorescence polarization was immediately measured. (C) T119M TTR (white), M-TTR (gray), or V30M M-TTR (black) at 0.2 mg/mL was incubated in 200 mM acetate buffer, pH 4.8, 37 °C, in the presence of 20 μg/mL fluoresceinated heparin, and the fluorescence polarization was measured as a function of time.

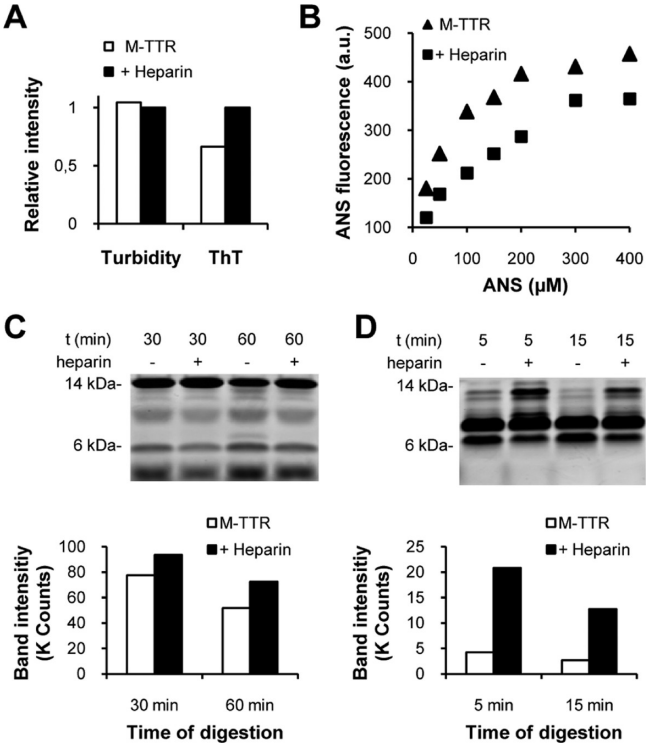

FIGURE 9: Influence of heparin on the structural properties of aggregates derived from M-TTR. (A) M-TTR aggregates grown for 5 days at pH 4.8, 37 °C, in the absence (white) or presence (black) of 20 μg/mL heparin and isolated by centrifugation were resuspended in buffer A at a final concentration of 0.2 mg/mL, and the absorbance at 400 nm (turbidity) was measured as well as the ThT fluorescence in the presence of 20 μM ThT. Results are expressed relative to the M-TTR fibrils obtained in the presence of heparin (black bars assigned to be unity) monitored by either ThT fluorescence or turbidity. (B) ANS binding to 0.2 mg/mL M-TTR aggregates prepared in the absence (▲) or presence (■) of 20 μg/mL heparin. The ANS fluorescence intensity was measured at 470 nm. (C) Trypsin digestion of M-TTR aggregates formed in the absence or presence of heparin (20 μg/mL). Aggregates were incubated with trypsin at an enzyme-to-substrate ratio of 1:200 (w/w) at 37 °C for 30 or 60 min and then analyzed by SDS−PAGE. The bands corresponding to uncleaved M-TTR (14 kDa) detected by Coomassie blue staining were quantified (bottom). (D) Proteinase K digestion of M-TTR aggregates formed in the absence or presence of heparin. Aggregates were incubated with proteinase K at a ratio of 1:2000 (w/w) at 25 °C for 5 or 15 min and then analyzed by SDS−PAGE. The bands corresponding to a high molecular weight M-TTR fragment (≈13 kDa) detected by Coomassie blue staining were quantified (bottom).

with heparin is lower than that obtained without heparin at equivalent ANS concentrations (Figure 9B), indicating that aggregates grown with heparin have a lower degree of exposure of solvent-accessible hydrophobic clusters. Limited proteolysis of TTR aggregates was accomplished using trypsin and proteinase K and investigated by SDS−PAGE and LC-MS. TTR aggregates are known to disassemble into monomers (14 kDa) after boiling in SDS-loading buffer. Therefore, monomer band intensity is indicative of TTR monomers making up the aggregates that remained uncleaved after protease treatment. After trypsin digestion, the 14 kDa band corresponding to nondigested M-TTR was more intense in the case of aggregates grown in the presence of heparin compared to those grown in the absence of heparin (Figure 9C). Analysis of trypsin-digested products by LC-MS revealed that the peptide fingerprints were identical for both types of aggregates, with the major fragments being Val^{71}−Glu^{127} (6325 Da) and Thr^{49}−Lys^{76} (3141 Da). In an analogous but more dramatic experiment, the presence of heparin also protected TTR aggregates from proteinase K digestion (Figure 9D). The proteolytic peptide fingerprints were similar with and without heparin (Figure 9D). These results demonstrate that the presence of heparin enhances the resistance of M-TTR aggregates to trypsin and proteinase K proteolysis. That the peptide fingerprints generated by trypsin and proteinase K digestion were similar in the presence and absence of heparin suggests that heparin is not enhancing protease resistance by

shielding specific cleavage sites but rather by protecting the overall protein through alteration of the quaternary structure of the aggregates, consistent with the results obtained from ANS and ThT fluorescence.

Unlike some amyloidogenic proteins whose aggregation is readily followed by electron miscroscopy and/or atomic force microscopy (AFM), TTR forms cross-β-sheet-rich aggregates that do not exhibit long-range order, and thus, well-defined amyloid fibrils are not formed. Nonetheless, utilization of AFM allowed us to demonstrate that TTR formed larger aggregates in the presence of heparin (pH 4.8, 37 °C) vs in its absence 1 h into an aggregation time course (Supporting Information Figure S6). These differences were not as obvious 30 min into the aggregation time course (Supporting Information Figure S6) but were still discernible. Sampling beyond 1 h into the TTR aggregation time course leads to the formation of massive and very heterogeneous aggregates that are very challenging to image.

DISCUSSION

GAGs are found to be closely associated with all amyloid fibrils isolated from humans (*17*). Biophysical studies have shown that GAGs accelerate the fibrillogenesis of both intrinsically disordered proteins and proteins that initially adopt a well-defined structure, like TTR. These observations suggest that GAGs could play an active role in amyloidogenesis *in vivo*, perhaps even a protective role, by quaternary structural conversion of proteotoxic soluble oligomers into less toxic amyloid fibrils and related cross-β-sheet aggregates. While a variety of hypotheses have been put forward to explain the mechanisms by which GAGs facilitate amyloid fibril formation, scant mechanistic data are available, and the precise mechanism by which GAGs accelerate amyloidogenesis is subject to debate. Herein, we report the mechanistic basis by which sulfated GAGs accelerate TTR amyloidogenesis.

Among the various GAGs explored in the present study, heparin was most effective at accelerating WT TTR and engineered M-TTR acid-mediated aggregation. HS and chondroitin sulfate, previously found in association with TTR fibrils located in peripheral nerves and in the heart (*18*, *19*), were also potent inducers of TTR amyloidogenesis. Since different tissue ECMs comprise different GAGs, this result could provide insights into the tissue-specific deposition and tissue-selective proteotoxicity of certain TTR variants. The sulfate moieties of the GAGs are critical for maximal acceleration of amyloidogenesis. For example, the nonsulfated GAG, hyaluronic acid, was ineffective at accelerating TTR aggregation, whereas *N*-acetylheparin bearing up to two sulfate groups per disaccharide repeating unit was less efficient at accelerating amyloidogenesis than heparin with its three sulfate groups per disaccharide. These results are consistent with previous studies focused on other amyloidogenic polypeptides (*25*, *27*, *64*, *65*) and confirm the key role that the sulfated structure of GAGs plays in accelerating amyloid fibril formation. The polymeric nature of GAGs was also essential for hastening TTR aggregation. This size-dependent effect, which has been previously reported for gelsolin (*25*), Aβ (*64*), and mAcP (*31*), is likely related to the capacity of larger GAGs to interact with multiple aggregates simultaneously, accelerating the formation of larger aggregates through a scaffold-based quaternary structure conversion mechanism.

We also demonstrated herein that the propensity of GAGs to accelerate TTR aggregation is dependent on electrostatic interactions between the negatively charged sulfate moieties composing the linear polysaccharides and the positive charges presented on the surface of TTR aggregates. The importance of the electrostatic interactions is demonstrated by the pH and salt dependence of the interaction between TTR aggregates and heparin. Heparin did not considerably accelerate the aggregation of amyloidogenic variants at pHs higher than 5.6 over a 30 h time course, although fibrillation was observed in aggregated samples without heparin. These results emphasize the importance of the positive net charge on TTR oligomers for efficient heparin-induced quaternary structural conversion. Similarly, it has been reported that the ability of GAGs to bind to Aβ(1−28) and Aβ(1−40) is also pH dependent (*72*) and that the binding of heparin to IAPP exhibits a higher affinity at low pH due to histidine protonation (*73*), supporting the importance of electrostatic interactions.

The weak interaction between TTR and heparin at neutral pH, also reported for other amyloidogenic proteins, underlines some concerns about the physiological relevance of the observed effects of GAGs on amyloidogenesis. As shown by fluorescence polarization, heparin did interact with M-TTR oligomers at pH 7.6, although this interaction did not seem to accelerate amyloidogenesis over the 30 h time course. Nonetheless, the weak interaction between GAGs and TTR oligomers taking place under the neutral pH conditions prevailing in the ECM could influence TTR deposition by locally increasing TTR oligomer concentration, facilitating the quaternary structural conversion of smaller aggregates into larger aggregates, including amyloid fibrils.

One of the main unsolved issues concerning the elucidation of the precise mechanism(s) of GAG-accelerated amyloidogenesis is whether GAGs mediate the association of monomeric proteins and/or already formed aggregates. The present data strongly suggest that GAGs preferentially interact with preformed TTR aggregates. First, when M-TTR pH-mediated aggregation was monitored by turbidity at 400 nm and by light scattering at 90°, the initial increase in signal intensity did not occur earlier in the presence of heparin, suggesting that GAGs act by enhancing the self-assembly of preformed aggregates, rather than accelerating the dissociation or increasing the population of amyloidogenic monomers. The sharp increase in ThT fluorescence observed after the addition of heparin later in the time course of the aggregation reaction appears to be explained by a quaternary structural conversion to higher molecular weight aggregates. The red shift of the β-sheet minimum observed by CD spectroscopy, the increased resistance to limited proteolysis, the lower ANS fluorescence, and the higher ThT fluorescence reported for TTR aggregates grown in the presence of heparin together suggest that heparin affects the quaternary structure of the aggregates.

Second, by employing fluoresceinated heparin, we observed that the increase of fluorescence polarization in aggregating samples at pH 4.8 or 5.2 was always preceded by ThT fluorescence, indicating that heparin most likely binds to ThT-positive species with some cross-β-sheet structure. Third, fluoresceinated heparin interacted with TTR oligomers, large soluble aggregates, and fibrils at pH 4.8, but notably not with native M-TTR monomers or WT TTR tetramers. At pH 7.6, heparin could bind to oligomers but not to other TTR species, probably because oligomers are relatively unstructured and thus expose more positive charge. Fourth, dynamic light scattering revealed that heparin did not increase the size of the initial aggregates formed during the first 30 min of incubation but rather stimulated the formation of larger aggregates that remained in solution

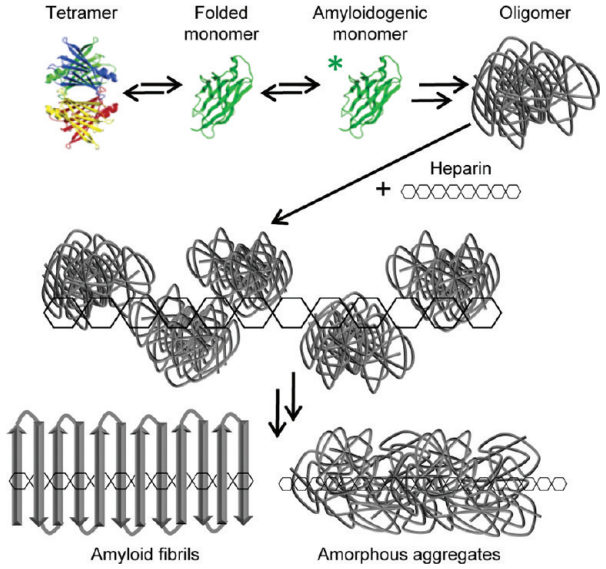

FIGURE 10: Schematic representation of the proposed mechanism by which sulfated glycosaminoglycans accelerate transthyretin amyloidogenesis. In the proposed mechanism supported by our data, as described in the text, GAGs do not influence the initial steps of the TTR amyloidogenesis cascade, including tetramer dissociation, partial misfolding of the released monomer to form the amyloidogenic monomer, or the initial formation of TTR oligomers. Instead, the sulfated polymeric surface of GAGs interacts with TTR oligomers, primarily through electrostatic interactions, concentrating TTR oligomers and possibly orienting them so as to accelerate the formation of larger aggregates by quaternary structural conversion.

after 120 min. By means of analytical size exclusion chromatography, we also observed that heparin accelerated the disappearance of soluble aggregates (>100 kDa) by inducing the formation of larger aggregates that were removed through 0.22 μm filtration. Moreover, by using AFM, we observed that heparin induced the formation of larger aggregates 60 min into the aggregation time course, relative to the corresponding sample in the absence of heparin. Taken together, these results suggest that heparin stimulates TTR amyloidogenesis mainly by facilitating the self-assembly of preformed aggregates into larger aggregates with an altered quaternary structure by means of a templated quaternary structural conversion mechanism (Figure 10), enabled by concentrating and likely orienting oligomers. Although our data strongly support this hypothesis, we cannot exclude the possibility that heparin could also accelerate TTR amyloidogenesis by mediating the oligomerization of misfolded monomeric M-TTR, as previously reported for mAcP (*36*), although we would submit that the more rapid disappearance of the monomer is due to the linked equilibria described above.

In conclusion, the present study reveals that sulfated GAGs, especially heparin, accelerate TTR aggregation through a scaffolding-based quaternary structural conversion mechanism involving electrostatic interactions between TTR aggregates and the sulfate moieties on polymeric GAGs. The high density of sulfate groups and the polymeric nature of GAGs seem to be essential for binding to multiple TTR oligomers simultaneously and converting them into higher molecular weight aggregates (Figure 10), possibly by preferentially aligning them. The presence of heparin in the TTR aggregation reaction appears to afford a more ordered high molecular weight aggregate structure that exhibits increased proteolysis resistance, as well as a lower exposure of hydrophobic side chains. Although the conditions employed in this study may not faithfully reproduce the complex environment prevailing in the ECM of humans, these results suggest that GAGs likely play a role in the TTR amyloidoses and may contribute to the distinct tissue selectivity of TTR amyloid diseases, which seems to be determined by the sequence of TTR that is inherited. That heparin interacts preferentially with TTR oligomers represents an important piece of the puzzle to better understand how GAGs accelerate amyloidogenesis. Since oligomers of various amyloidogenic proteins have been hypothesized to be the most proteotoxic species, it could be envisaged that GAGs play a protective role by interacting with toxic oligomers, facilitating their quaternary structural conversion into less proteotoxic amyloid fibrils.

ACKNOWLEDGMENT

We thank Colleen Fearns for careful reading and editing of the manuscript, Evan Powers for helpful discussions, and the reviewers for making this a better manuscript.

SUPPORTING INFORMATION AVAILABLE

Effect of glycosaminoglycans on WT TTR and M-TTR aggregation; effect of heparin on A25T TTR aggregation kinetics; effect of heparin on A25T TTR, V30M TTR, and V30M M-TTR aggregation kinetics; dependence of acid-mediated M-TTR conformational change on M-TTR concentration; interactions of TTR with heparin measured by fluorescence polarization of fluorescein-labeled heparin; effect of heparin on M-TTR aggregation monitored by AFM. This material is available free of charge via the Internet at http://pubs.acs.org.

REFERENCES

1. Buxbaum, J. N. (2004) The systemic amyloidoses. *Curr. Opin. Rheumatol. 16*, 67–75.
2. Chiti, F., and Dobson, C. M. (2006) Protein misfolding, functional amyloid, and human disease. *Annu. Rev. Biochem. 75*, 333–366.
3. Kelly, J. W. (1998) The alternative conformations of amyloidogenic proteins and their multi-step assembly pathways. *Curr. Opin. Struct. Biol. 8*, 101–106.
4. Dobson, C. M. (2003) Protein folding and misfolding. *Nature 426*, 884–890.
5. Cohen, F. E., and Kelly, J. W. (2003) Therapeutic approaches to protein-misfolding diseases. *Nature 426*, 905–909.
6. Sekijima, Y., Wiseman, R. L., Matteson, J., Hammarström, P., Miller, S. R., Sawkar, A. R., Balch, W. E., and Kelly, J. W. (2005) The biological and chemical basis for tissue-selective amyloid disease. *Cell 121*, 73–85.
7. Selkoe, D. J. (2003) Folding proteins in fatal ways. *Nature 426*, 900–904.
8. Johnson, S. M., Wiseman, R. L., Sekijima, Y., Green, N. S., Adamski-Werner, S. L., and Kelly, J. W. (2005) Native state kinetic stabilization as a strategy to ameliorate protein misfolding diseases: a focus on the transthyretin amyloidoses. *Acc. Chem. Res. 38*, 911–921.
9. Kayed, R., Head, E., Thompson, J. L., McIntire, T. M., Milton, S. C., Cotman, C. W., and Glabe, C. G. (2003) Common structure of soluble amyloid oligomers implies common mechanism of pathogenesis. *Science 300*, 486–489.
10. Reixach, N., Deechongkit, S., Jiang, X., Kelly, J. W., and Buxbaum, J. N. (2004) Tissue damage in the amyloidoses: transthyretin monomers and nonnative oligomers are the major cytotoxic species in tissue culture. *Proc. Natl. Acad. Sci. U.S.A. 101*, 2817–2822.
11. Lambert, M. P., Barlow, A. K., Chromy, B. A., Edwards, C., Freed, R., Liosatos, M., Morgan, T. E., Rozovsky, I., Trommer, B., Viola, K. L., Wals, P., Zhang, C., Finch, C. E., Krafft, G. A., and Klein, W. L. (1998) Diffusible, nonfibrillar ligands derived from Abeta1−42 are potent central nervous system neurotoxins. *Proc. Natl. Acad. Sci. U.S.A. 95*, 6448–6453.
12. Townsend, M., Shankar, G. M., Mehta, T., Walsh, D. M., and Selkoe, D. J. (2006) Effects of secreted oligomers of amyloid beta-protein on hippocampal synaptic plasticity: a potent role for trimers. *J. Physiol. 572*, 477–492.

13. Demuro, A., Mina, E., Kayed, R., Milton, S. C., Parker, I., and Glabe, C. G. (2005) Calcium dysregulation and membrane disruption as a ubiquitous neurotoxic mechanism of soluble amyloid oligomers. *J. Biol. Chem. 280*, 17294–17300.
14. Pepys, M. B., Booth, D. R., Hutchinson, W. L., Gallimore, J. R., Collins, P. M., and Hohenester, E. (1997) Amyloid P component: a critical review. *Amyloid: Int. J. Exp. Clin. Invest. 4*, 274–295.
15. Alexandrescu, A. T. (2005) Amyloid accomplices and enforcers. *Protein Sci. 14*, 1–12.
16. Kisilevsky, R. (2000) The relation of proteoglycans, serum amyloid P and apo E to amyloidosis current status. *Amyloid 7*, 23–25.
17. Ancsin, J. B. (2003) Amyloidogenesis: historical and modern observations point to heparan sulfate proteoglycans as a major culprit. *Amyloid 10*, 67–79.
18. Magnus, J. H., Stenstad, T., Kolset, S. O., and Husby, G. (1991) Glycosaminoglycans in extracts of cardiac amyloid fibrils from familial amyloid cardiomyopathy of Danish origin related to variant transthyretin Met 111. *Scand. J. Immunol. 34*, 63–69.
19. Inoue, S., Kuroiwa, M., Saraiva, M. J., Guimarães, A., and Kisilevsky, R. (1998) Ultrastructure of familial amyloid polyneuropathy amyloid fibrils: examination with high-resolution electron microscopy. *J. Struct. Biol. 124*, 1–12.
20. DeWitt, D. A., Silver, J., Canning, D. R., and Perry, G. (1993) Chondroitin sulfate proteoglycans are associated with the lesions of Alzheimer's disease. *Exp. Neurol. 121*, 149–152.
21. Ohishi, H., Skinner, M., Sato-Araki, N., Okuyama, T., Gejyo, F., Kimura, A., Cohen, A. S., and Schmid, K. (1990) Glycosaminoglycans of the hemodialysis-associated carpal synovial amyloid and of amyloid-rich tissues and fibrils of heart, liver, and spleen. *Clin. Chem. 36*, 88–91.
22. Stenstad, T., Magnus, J. H., Kolset, S. O., Cornwell, G. G., and Husby, G. (1991) Macromolecular properties of glycosaminoglycans in primary AL amyloid fibril extracts of lymphoid tissue origin. *Scand. J. Immunol. 34*, 611–617.
23. Young, I. D., Ailles, L., Narindrasorasak, S., Tan, R., and Kisilevsky, R. (1992) Localization of the basement membrane heparan sulfate proteoglycan in islet amyloid deposits in type II diabetes mellitus. *Arch. Pathol. Lab. Med. 116*, 951–954.
24. Pérez, M., Wandosell, F., Colaço, C., and Avila, J. (1998) Sulphated glycosaminoglycans prevent the neurotoxicity of a human prion protein fragment. *Biochem. J. 335*, 369–374.
25. Suk, J. Y., Zhang, F., Balch, W. E., Linhardt, R. J., and Kelly, J. W. (2006) Heparin accelerates gelsolin amyloidogenesis. *Biochemistry 45*, 2234–2242.
26. McLaughlin, R. W., De Stigter, J. K., Sikkink, L. A., Baden, E. M., and Ramirez-Alvarado, M. (2006) The effects of sodium sulfate, glycosaminoglycans, and Congo red on the structure, stability, and amyloid formation of an immunoglobulin light-chain protein. *Protein Sci. 15*, 1710–1722.
27. McLaurin, J., Franklin, T., Zhang, X., Deng, J., and Fraser, P. E. (1999) Interactions of Alzheimer amyloid-beta peptides with glycosaminoglycans effects on fibril nucleation and growth. *Eur. J. Biochem. 266*, 1101–1110.
28. Cohlberg, J. A., Li, J., Uversky, V. N., and Fink, A. L. (2002) Heparin and other glycosaminoglycans stimulate the formation of amyloid fibrils from alpha-synuclein in vitro. *Biochemistry 41*, 1502–1511.
29. Yamamoto, S., Hasegawa, K., Yamaguchi, I., Goto, Y., Gejyo, F., and Naiki, H. (2005) Kinetic analysis of the polymerization and depolymerization of beta(2)-microglobulin-related amyloid fibrils in vitro. *Biochim. Biophys. Acta 1753*, 34–43.
30. Meng, F., Abedini, A., Song, B., and Raleigh, D. P. (2007) Amyloid formation by pro-islet amyloid polypeptide processing intermediates: examination of the role of protein heparan sulfate interactions and implications for islet amyloid formation in type 2 diabetes. *Biochemistry 46*, 12091–12099.
31. Motamedi-Shad, N., Monsellier, E., and Chiti, F. (2009) Amyloid formation by the model protein muscle acylphosphatase is accelerated by heparin and heparan sulphate through a scaffolding-based mechanism. *J. Biochem. 146*, 805–814.
32. Relini, A., De Stefano, S., Torrassa, S., Cavalleri, O., Rolandi, R., Gliozzi, A., Giorgetti, S., Raimondi, S., Marchese, L., Verga, L., Rossi, A., Stoppini, M., and Bellotti, V. (2008) Heparin strongly enhances the formation of beta2-microglobulin amyloid fibrils in the presence of type I collagen. *J. Biol. Chem. 283*, 4912–4920.
33. Yamamoto, S., Yamaguchi, I., Hasegawa, K., Tsutsumi, S., Goto, Y., Gejyo, F., and Naiki, H. (2004) Glycosaminoglycans enhance the trifluoroethanol-induced extension of beta 2-microglobulin-related amyloid fibrils at a neutral pH. *J. Am. Soc. Nephrol. 15*, 126–133.
34. Myers, S. L., Jones, S., Jahn, T. R., Morten, I. J., Tennent, G. A., Hewitt, E. W., and Radford, S. E. (2006) A systematic study of the effect of physiological factors on beta2-microglobulin amyloid formation at neutral pH. *Biochemistry 45*, 2311–2321.
35. Yamaguchi, I., Suda, H., Tsuzuike, N., Seto, K., Seki, M., Yamaguchi, Y., Hasegawa, K., Takahashi, N., Yamamoto, S., Gejyo, F., and Naiki, H. (2003) Glycosaminoglycan and proteoglycan inhibit the depolymerization of beta2-microglobulin amyloid fibrils in vitro. *Kidney Int. 64*, 1080–1088.
36. Motamedi-Shad, N., Monsellier, E., Torrassa, S., Relini, A., and Chiti, F. (2009) Kinetic analysis of amyloid formation in the presence of heparan sulfate: faster unfolding and change of pathway. *J. Biol . Chem. 284*, 29921–29934.
37. McCubbin, W. D., Kay, C. M., Narindrasorasak, S., and Kisilevsky, R. (1988) Circular-dichroism studies on two murine serum amyloid A proteins. *Biochem. J. 256*, 775–783.
38. Andrade, C. (1952) A peculiar form of peripheral neuropathy; familiar atypical generalized amyloidosis with special involvement of the peripheral nerves. *Brain 75*, 408–427.
39. Jacobson, D. R., Pastore, R. D., Yaghoubian, R., Kane, I., Gallo, G., Buck, F. S., and Buxbaum, J. N. (1997) Variant-sequence transthyretin (isoleucine 122) in late-onset cardiac amyloidosis in black Americans. *N. Engl. J. Med. 336*, 466–473.
40. Connelly, S., Choi, S., Johnson, S. M., Kelly, J. W., and Wilson, I. A. (2010) Structure-based design of kinetic stabilizers that ameliorate the transthyretin amyloidoses. *Curr. Opin. Struct. Biol. 20*, 54–62.
41. Blake, C. C., Geisow, M. J., Oatley, S. J., Rérat, B., and Rérat, C. (1978) Structure of prealbumin: secondary, tertiary and quaternary interactions determined by Fourier refinement at 1.8 Å. *J. Mol. Biol. 121*, 339–356.
42. Buxbaum, J. N., and Reixach, N. (2009) Transthyretin: the servant of many masters. *Cell. Mol. Life Sci. 66*, 3095–3101.
43. Westermark, P., Sletten, K., Johansson, B., and Cornwell, G. G. (1990) Fibril in senile systemic amyloidosis is derived from normal transthyretin. *Proc. Natl. Acad. Sci. U.S.A. 87*, 2843–2845.
44. Saraiva, M. J. (2001) Transthyretin mutations in hyperthyroxinemia and amyloid diseases. *Hum. Mutat. 17*, 493–503.
45. Mitsuhashi, S., Yazaki, M., Tokuda, T., Sekijima, Y., Washimi, Y., Shimizu, Y., Ando, Y., Benson, M. D., and Ikeda, S. (2005) Biochemical characteristics of variant transthyretins causing hereditary leptomeningeal amyloidosis. *Amyloid 4*, 216–225.
46. Jacobson, D. R., McFarlin, D. E., Kane, I., and Buxbaum, J. N. (1992) Transthyretin Pro55, a variant associated with early-onset, aggressive, diffuse amyloidosis with cardiac and neurologic involvement. *Hum. Genet. 89*, 353–356.
47. Colon, W., and Kelly, J. W. (1992) Partial denaturation of transthyretin is sufficient for amyloid fibril formation in vitro. *Biochemistry 31*, 8654–8660.
48. Kelly, J. W., Colon, W., Lai, Z., Lashuel, H. A., McCulloch, J., McCutchen, S. L., Miroy, G. J., and Peterson, S. A. (1997) Transthyretin quaternary and tertiary structural changes facilitate misassembly into amyloid. *Adv. Protein Chem. 50*, 161–181.
49. Foss, T. R., Wiseman, R. L., and Kelly, J. W. (2005) The pathway by which the tetrameric protein transthyretin dissociates. *Biochemistry 44*, 15525–15533.
50. Lai, Z., Colón, W., and Kelly, J. W. (1996) The acid-mediated denaturation pathway of transthyretin yields a conformational intermediate that can self-assemble into amyloid. *Biochemistry 35*, 6470–6482.
51. Hammarström, P., Wiseman, R. L., Powers, E. T., and Kelly, J. W. (2003) Prevention of transthyretin amyloid disease by changing protein misfolding energetics. *Science 299*, 713–716.
52. Jiang, X., Smith, C. S., Petrassi, H. M., Hammarström, P., White, J. T., Sacchettini, J. C., and Kelly, J. W. (2001) An engineered transthyretin monomer that is nonamyloidogenic, unless it is partially denatured. *Biochemistry 40*, 11442–11452.
53. Hurshman, A. R., White, J. T., Powers, E. T., and Kelly, J. W. (2004) Transthyretin aggregation under partially denaturing conditions is a downhill polymerization. *Biochemistry 43*, 7365–7381.
54. Hammarström, P., Jiang, X., Hurshman, A. R., Powers, E. T., and Kelly, J. W. (2002) Sequence-dependent denaturation energetics: a major determinant in amyloid disease diversity. *Proc. Natl. Acad. Sci. U.S.A. 99*, 16427–16432.
55. Hurshman Babbes, A. R., Powers, E. T., and Kelly, J. W. (2008) Quantification of the thermodynamically linked quaternary and tertiary structural stabilities of transthyretin and its disease-associated variants: the relationship between stability and amyloidosis. *Biochemistry 47*, 6969–6984.
56. McCutchen, S. L., Lai, Z., Miroy, G. J., Kelly, J. W., and Colón, W. (1995) Comparison of lethal and nonlethal transthyretin variants

and their relationship to amyloid disease. *Biochemistry 34*, 13527–13536.
57. Sousa, M. M., and Saraiva, M. J. (2003) Neurodegeneration in familial amyloid polyneuropathy: from pathology to molecular signaling. *Prog. Neurobiol. 71*, 385–400.
58. Sawabe, M., Hamamatsu, A., Ito, T., Arai, T., Ishikawa, K., Chida, K., Izumiyama, N., Honma, N., Takubo, K., and Nakazato, M. (2003) Early pathogenesis of cardiac amyloid deposition in senile systemic amyloidosis: close relationship between amyloid deposits and the basement membranes of myocardial cells. *Virchows Arch. 442*, 252–257.
59. Glabe, C. G., Harty, P. K., and Rosen, S. D. (1983) Preparation and properties of fluorescent polysaccharides. *Anal. Biochem. 130*, 287–294.
60. Naiki, H., Higuchi, K., Hosokawa, M., and Takeda, T. (1989) Fluorometric determination of amyloid fibrils in vitro using the fluorescent dye, thioflavin T1. *Anal. Biochem. 177*, 244–249.
61. Lindahl, U., and Höök, M. (1978) Glycosaminoglycans and their binding to biological macromolecules. *Annu. Rev. Biochem. 47*, 385–417.
62. Monsellier, E., Ramazzotti, M., Taddei, N., and Chiti, F. (2010) A computational approach for identifying the chemical factors involved in the glycosaminoglycans-mediated acceleration of amyloid fibril formation. *PLoS One 5*, e11363.
63. Castillo, G. M., Cummings, J. A., Yang, W., Judge, M. E., Sheardown, M. J., Rimvall, K., Hansen, J. B., and Snow, A. D. (1998) Sulfate content and specific glycosaminoglycan backbone of perlecan are critical for perlecan's enhancement of islet amyloid polypeptide (amylin) fibril formation. *Diabetes 47*, 612–620.
64. Fraser, P. E., Darabie, A. A., and McLaurin, J. A. (2001) Amyloid-beta interactions with chondroitin sulfate-derived monosaccharides and disaccharides, implications for drug development. *J. Biol. Chem. 276*, 6412–6419.
65. Calamai, M., Kumita, J. R., Mifsud, J., Parrini, C., Ramazzotti, M., Ramponi, G., Taddei, N., Chiti, F., and Dobson, C. M. (2006) Nature and significance of the interactions between amyloid fibrils and biological polyelectrolytes. *Biochemistry 45*, 12806–12815.
66. Dember, L. M., Hawkins, P. N., Hazenberg, B. P., Gorevic, P. D., Merlini, G., and Butrimiene, I. (2007) Eprodisate for the treatment of renal disease in AA amyloidosis. *N. Engl. J. Med. 356*, 2349–2360.
67. Aisen, P. S., Gauthier, S., Vellas, B., Briand, R., Saumier, D., Laurin, J., and Garceau, D. (2007) Alzhemed: a potential treatment for Alzheimer's disease. *Curr. Alzheimer Res. 4*, 473–478.
68. Hammarström, P., Schneider, F., and Kelly, J. W. (2001) Trans-suppression of misfolding in an amyloid disease. *Science 293*, 2459–2462.
69. Lashuel, H. A., Lai, Z., and Kelly, J. W. (1998) Characterization of the transthyretin acid denaturation pathways by analytical ultracentrifugation: implications for wild-type, V30M, and L55P amyloid fibril formation. *Biochemistry 37*, 17851–17964.
70. Jiang, X., Buxbaum, J. N., and Kelly, J. W. (2001) The V122I cardiomyopathy variant of transthyretin increases the velocity of rate-limiting tetramer dissociation, resulting in accelerated amyloidosis. *Proc. Natl. Acad. Sci. U.S.A. 98*, 14943–14948.
71. Cardamone, M., and Puri, N. K. (1992) Spectrofluorimetric assessment of the surface hydrophobicity of proteins. *Biochem. J. 282*, 589–593.
72. Brunden, K. R., Richter-Cook, N. J., Chaturvedi, N., and Frederickson, R. C. (1993) pH-dependent binding of synthetic beta-amyloid peptides to glycosaminoglycans. *J. Neurochem. 61*, 2147–2154.
73. Abedini, A., Tracz, S. M., Cho, J. H., and Raleigh, D. P. (2006) Characterization of the heparin binding site in the N-terminus of human pro-islet amyloid polypeptide: implications for amyloid formation. *Biochemistry 45*, 9228–9237.